© 2021. Published by The Company of Biologists Ltd | Journal of Cell Science (2021) 134, jcs250720. doi:10.1242/jcs.250720

RESEARCH ARTICLE

Characterization of human bone marrow niches with metabolome and transcriptome profiling

Selda Ayhan[1,2], Emirhan Nemutlu[3], Duygu Uçkan Çetinkaya[1,4], Sedef Kır[3] and Rıza Köksal Özgül[2,*]

ABSTRACT

Bone marrow (BM) niches are special microenvironments that work in harmony with each other for the regulation and maintenance of hematopoiesis. Niche investigations have thus far been limited to various model organisms and animal studies; therefore, little is known about different niches in healthy humans. In this study, a special harvesting method for the collection of BM from two different anatomical regions in the iliac crest of humans was used to investigate the presence of different niches in BM. Additionally, metabolomic and transcriptomic profiles were compiled using comparative 'omics' technologies, and the main cellular pathways and corresponding transcripts and metabolites were identified. As a result, we found that the energy metabolism between the regions was different. This study provides basic broad data for regenerative medicine in terms of the design of the appropriate microenvironment for *in vitro* hematopoietic niche modeling, and identifies the normal reference values that can be compared in hematological disease.

KEY WORDS: Bone marrow, Niche, Mesenchymal stem cells, Hematopoietic stem cells, Metabolomics, Transcriptomics

INTRODUCTION

Hematopoiesis is a production process of all mature blood cell types that arise from hematopoietic stem cells (HSCs). Bone marrow (BM) is the major site of hematopoiesis in adults. HSCs have the capacity for self-renewal, ability of differentiation and proliferation into lineage-committed and multipotential progenitor cells. Highly specialized microenvironments that enable all of these hierarchical hematopoiesis pathways (self-renewal, differentiation, proliferation and migration) to work in tremendous harmony in the same BM are called 'niche' (Nagasawa et al., 2011; Park et al., 2012; Szade et al., 2018; Tjin et al., 2019; Wei and Frenette, 2018). The concept of a niche in the BM was first proposed by Schofield (1978), and it has gained widespread popularity. Although the concept of the 'niche' is well accepted, it remains poorly understood. Until today, many investigators have tried to untangle which cell types constitute and organize niches, what are their functions, and how the same type of stromal cells assume distinct functions when they settle in different niches (Crane et al., 2017; Gao et al., 2018).

Most of the literature regarding the stem cell niche comes from studies in various model organisms and animals; there is no literature about humans, until this study. BM is not a solid tissue, and it is very difficult to study and define BM hematopoietic niches even in animal studies. So far, in those studies, different techniques and methods, such as *ex vivo*, intravital, quantitative imaging (Cordeiro Spinetti et al., 2015; Nombela-Arrieta et al., 2013; Sudo and Mizuno, 2018; Tjin et al., 2019; Winkler et al., 2010; Xie et al., 2009) and collagenase digestion (Balduino et al., 2012; Grassinger et al., 2010; Hu et al., 2016; Patterson et al., 2017) have been used to determine and show the anatomical boundaries, cell populations and function of niches. In humans, a BM biopsy sample would be more informative for the characterization of the different marrow niches. However, in standard BM harvest practice for transplantation purposes, multiple BM aspirations are performed, and taking a BM biopsy for research is not an option. Also, even for BM aspiration, rather than biopsy, there is no optimized sample collection technique to distinguish anatomical borders of different niches, as it is not a part of standard practice during BM collection.

According to the experiments in model organisms and animals, there are basically two different niches, including endosteal (also called osteoblastic) and vascular (also called perisinusoidal) niches in the BM. Both niches work in harmony to maintain hematopoietic homeostasis (Chotinantakul and Leeanansaksiri, 2012; Guerrouahen et al., 2011; Lilly et al., 2011). Studies have indicated that the osteoblast-rich endosteal niche localized fairly close to the bone cortex is the region in which HSCs are kept in a quiescent state for a long time. It has been hypothesized that this site is hypoxic and rich in calcium associated with parathyroid hormone activation and sympathetic nervous system innervation. It has been suggested that this specialized immune-privileged microenvironment protects stem cells from toxic and immune insults by keeping them in a silent state by suppressing cell cycle entry. Whereas the vascular niche, which is rich in blood vessels, is thought to be responsible for the proliferation and differentiation of HSCs. It is speculated that when stressed or when hematopoiesis is needed, HSCs migrate from endosteal niches to a vascular niche and differentiate as a consequence of the interaction with the microenvironment of the vascular region (Anthony and Link, 2014; Crane et al., 2017; Lilly et al., 2011). In recent years, niche studies have focused on different types of vessels, such as arterioles and sinusoids in the BM. They have indicated that distinct vessels play a different role in hematopoiesis. The arteriolar niche localizes close to the bone cortex like the endosteal niche and often contains HSCs in the quiescent state, whereas the sinusoidal niches localize throughout the BM center and contain mostly hematopoietic progenitor cells (HPCs). The fenestrated basal lamina of the sinusoids provides the migration of differentiated HPCs from BM to peripheral blood. Therefore, reactive oxygen species (ROS) levels in the sinusoidal niche are higher than in the arteriolar niche

[1]Center for Stem Cell Research and Development/PEDI-STEM and Department of Stem Cell Sciences, Health Sciences Institute, Hacettepe University, Sıhhıye, Ankara 06100, Turkey. [2]Department of Pediatric Metabolism, Institute of Child Health, Hacettepe University, Sıhhıye, Ankara 06100, Turkey. [3]Faculty of Pharmacy, Department of Analytical Chemistry, Hacettepe University, Sıhhıye, Ankara 06100, Turkey. [4]Department of Pediatrics, Division of Hematology, Hacettepe University, Sıhhıye, Ankara 06100, Turkey.

*Author for correspondence (rkozgul@hacettepe.edu.tr)

S.A., 0000-0002-3525-7995; E.N., 0000-0002-7337-6215; D.U.C., 0000-0003-3593-6493; S.K., 0000-0003-1322-1665; R.K.Ö., 0000-0002-0283-635X

Handling Editor: Daniel Billadeau
Received 5 August 2020; Accepted 13 January 2021

Journal of Cell Science (2021) 134, jcs250720. doi:10.1242/jcs.250720

because exposure to blood plasma components is increased. Consistent with this, increased vascular permeability in the sinusoidal niche increases the mobilization of HSCs by reducing their quiescent state (Itkin et al., 2016; Klamer and Voermans, 2014).

The discovery of a healthy human BM niche will shed light on many human diseases, hematological disorders and malignancies in which the corrupted microenvironment is held responsible. BM niches have been reported to play a significant role in the onset and/or progression of hematopoietic malignancies, and niche studies have focused on this area (Wang and Zhong, 2018). In particular, the mesenchymal stem cells (MSCs), which are major components of niches, play a pivotal role in malignancies (Calvi and Link, 2015; Dias et al., 2002; Pleyer et al., 2016). In recent years, metabolic profiling of hematologic malignancies has become increasingly important in the discovery of biomarkers for diagnosis and treatment. In order to make comparisons, it is critically important to determine the BM metabolic profiles of healthy individuals. For technical or ethical reasons, it is still an important limitation, especially in the pediatric population (Tiziani et al., 2013). Similarly, *in vitro* mimicking of the BM microenvironment is crucial because of their potential to provide a continuous source of blood cells for transplantation, or to serve as an *in vitro* model to examine dysfunction in diseases and to investigate the action or toxicology of drugs on diseases. In spite of the use of biomaterials, microfluidic methods, three-dimensional cultures of different cell types and next-generation technologies, *ex vivo* hematopoietic expansion has remained a very challenging topic due to the difficulties in mimicking *in vivo* marrow microenvironment. Therefore, better identification and understanding of the human BM microenvironment are needed both in health and disease (Abarrategi et al., 2018; Sharma et al., 2012). Additionally, the influence of culture-induced metabolic changes on human MSC (hMSC) therapeutic potency is largely unknown. As the metabolic flow is extremely important in producing energy and anabolic molecules, determining the phenotypic and functional properties of cells, there is a need to illuminate the metabolic profiles of hMSCs used in therapeutic applications.

In this study, for the first time, the presence of different niches in healthy human BM was investigated. For this purpose, for the first time, in this study, the metabolomic and transcriptomic profiles of two anatomically different BM regions (superficial and deep aspirations) of healthy humans were defined separately by RNA-seq for transcriptomics and GC-MS for metabolomics. The presence of different niches in healthy human BM was investigated by the comparative analysis of defined metabolite and transcript pools. BW samples were obtained from two anatomically different regions of human BM, and experiments were performed in BM plasma samples, human bone marrow-derived mesenchymal stem cells (hBMSCs) and culture supernatants of passage 0 (P0) and passage 3 (P3) BMSCs. These aims may serve regenerative and clinic medicine in terms of the determination of the optimum requirements for *in vitro* cell culture media, design of the appropriate microenvironment for *in vitro* hematopoietic niche modeling, optimization of the methodologies for the collection of BM in transplantation, and providing reference values that can be compared in disease states, including hematologic malignancy and BM failure syndromes. Besides, this study represents a unique clinical resource for future research on the human BM niche.

RESULTS

The stromal cell concentration is higher in the region closer to the bone cortex than in the deeper region of the BM

Studies have demonstrated that most of the HSCs and stromal cells are concentrated in the endosteal niche of BM (Cordeiro Spinetti et al., 2015; Ehninger and Trumpp, 2011; Guezguez et al., 2013; Mendelson and Frenette, 2014; Muschler et al., 1997; Patterson et al., 2017; Sugiyama et al., 2006). To determine and compare the mononuclear cell (MNC) numbers in the R1 and R2 regions, and to dissect the effects of their cells on niche phenotype and function, we first isolated the MNCs and counted the total number of MNCs in each region (Fig. S1). The total number of MNCs isolated from R1 was higher than the R2 region (two sample paired *t*-test, P=0.01). There was a statistically significant negative correlation between the age and R1-MNC numbers of the donors (Pearson r=−0.716, P=0.01, two-tailed *t*-test, correlation is significant at the 0.01 level). There was not a correlation between age and R2-MNC numbers (Pearson r=−0.222, P=0.51, two-tailed *t*-test) (Fig. 1B).

However, to compare the typical cell characteristics of the MSCs isolated from MNCs, morphologies and proliferation capabilities of the cells in all progressive passages were observed under the inverted microscope. All of cultured cells exhibited characteristics of MSCs (fibroblastic spindle-shape, irregular-shaped and euchromatin nuclei, as well as rich inner cytoplasm; Miko et al., 2015). It was observed that the P0-hBMSCs isolated from the R1 region proliferated more rapidly than R2 by forming many colonies and reached 80% confluence in ∼9 days (Fig. 1C), but there was no difference in the proliferation speeds at progressive passages between regions.

To verify their identity, we characterized the immunophenotype and differentiation potential of hBMSC at P3. In the flow cytometry analysis, hBMSCs were positive for CD105, CD44, CD166, CD29, CD90, CD73 and HLA-ABC antibodies, but were negative for CD14, CD31, CD34, CD45 and HLA-DR. When R1 and R2-hBMSC were compared, there was no significant difference between the numbers of cells expressing these antigens (Fig. 2A). Then we focused on fluorescence intensity analysis of some antibodies that have been implicated in controlling the fate of HSCs in BM niches. Immunofluorescence staining was performed to determine the immunophenotypical characteristics of P3-hBMSCs obtained from R1 and R2 for MSC-associated markers CD29 (also known as integrin β1), CD44, fibronectin (FN, also known as FN1) and osteopontin (OPN, also known as SPP1). Fluorescence intensity of these antibody positive cells were higher in the R1 region than in R2 (Fig. 2B). The adipogenic and osteogenic differentiation potential of the cells were tested for 21 days. P3-hMSCs from both regions exhibited similar differentiation potentials (Fig. 2C).

Metabolite profile of BM plasma better reflects the *in vivo* microenvironment

The thought that plasma samples, rather than cultured cells, would better reflect the *in vivo* microenvironment prompted us to compare the plasma metabolomes of different anatomical regions by using an untargeted metabolomic approach (Fig. 3A). After metabolite profiles were obtained by GC-MS for the R1 and R2 regions, similarities or differences between these regions were investigated using comparative metabolite analysis. We detected and quantified 218 metabolites in plasma samples from GC-MC data. More detailed comparisons between the R1 and R2 regions were shown using partial least-squares discriminant analysis (PLS-DA) and regression coefficients analysis (Fig. 3B,C). Important metabolites that have the greatest effect at discriminating the two regions were determined via variable importance in projection (VIP) graphs, and which region contains more or less of which metabolite was determined using regression analysis. As a result of these comparative analyses, high amounts of statistically significant

Journal of Cell Science (2021) 134, jcs250720. doi:10.1242/jcs.250720

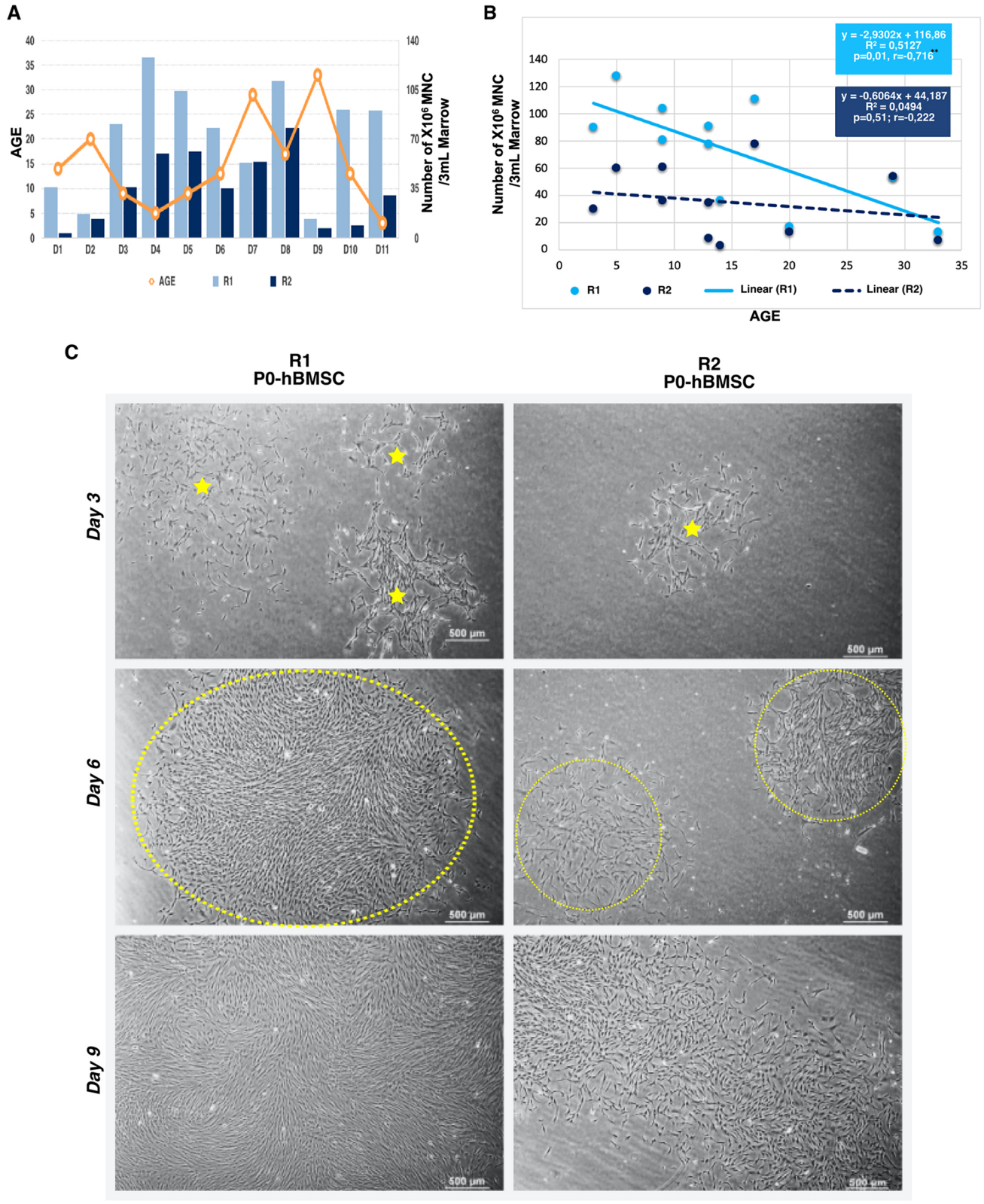

Fig. 1. MNCs isolated from the R1 region of BM versus R2 are more numerous and have higher proliferative potential. (A) Chart showing age with total MNC numbers in 3 ml BM samples aspirated from the R1 and R2 regions of each of 11 healthy BMT donors (*x*-axis, donor sets; D, donor). The total number of MNCs in the R1 region were higher than in the R2 region (two-sample paired *t*-test, P=0.01). (B) Representative correlation analysis plot between the donor's age with R1 region (light blue linear) and R2 region (dark blue linear) MNC counts. The correlation analysis was performed using Pearson's method and PASW Statistics software (version 18.0.0.). There is a statistically significant negative correlation between age and R1 MNC numbers (Pearson r=−0.716, P=0.01, two-tailed paired *t*-test). **P<0.01. No correlation between age and R2 MNC numbers (Pearson r=−0.222, P=0.51, two-tailed paired *t*-test) was observed. (C) Inverted microscope images of BM MSCs at P0 (P0-BMSC) on days 3, 6 and 9 of culture. Stars indicate the formed colonies on day 3 of culture. Yellow dashed lines indicate the borders of colonies (i.e. colony-size) on day 6 of culture. Scale bars: 500 µm.

Journal of Cell Science (2021) 134, jcs250720. doi:10.1242/jcs.250720

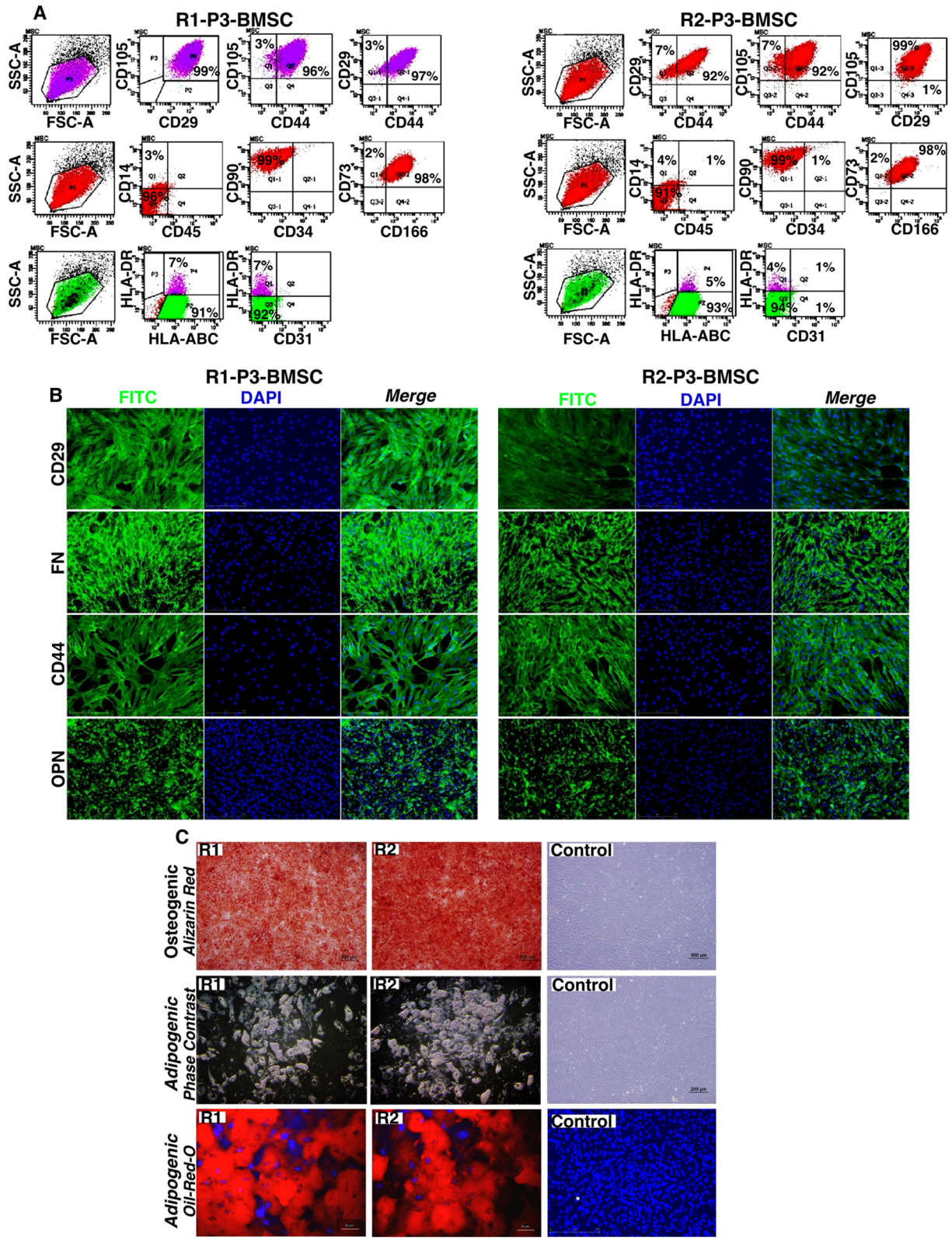

Fig. 2. Comparative characterization of P3-hBMSCs obtained from R1 and R2. (A) Flow cytometric characterization of BMSCs obtained from the R1 and R2 regions. P3-BMSCs of each region were identified as positive for CD105, CD44, CD166, CD29, CD90, CD73 and HLA-ABC antibodies, but negative for CD14, CD31, CD34, CD45 and HLA-DR. (B) Immunofluorescence staining demonstrating the existence of BM niche-associated markers CD29, CD44, FN and OPN in the P3-BMSC of R1 and R2 regions. In R2-BMSCs, all of the antibodies have weaker fluorescent intensity than R1. Magnification, 10×. (C) The adipogenic and osteogenic differentiation potentials of the hBMSCs from each region. In osteogenic differentiation, Alizarin Red staining identified the calcium nodules (red) secreted by induced osteoblasts. Magnification, 4×. In the phase-contrast microscope demonstrating lipid droplets of adipogenic differentiation the magnification is 10×. In adipogenic differentiation, Oil-Red-O (ORO) staining identified the neutral lipid droplets (red) (blue stain is DAPI). ORO magnification is 40×. Scale bars: 250 µm (B); 500 µm (C, Alizarin Red); 100 µm (C, phase contrast); 50 µm (C, ORO).

Journal of Cell Science (2021) 134, jcs250720. doi:10.1242/jcs.250720

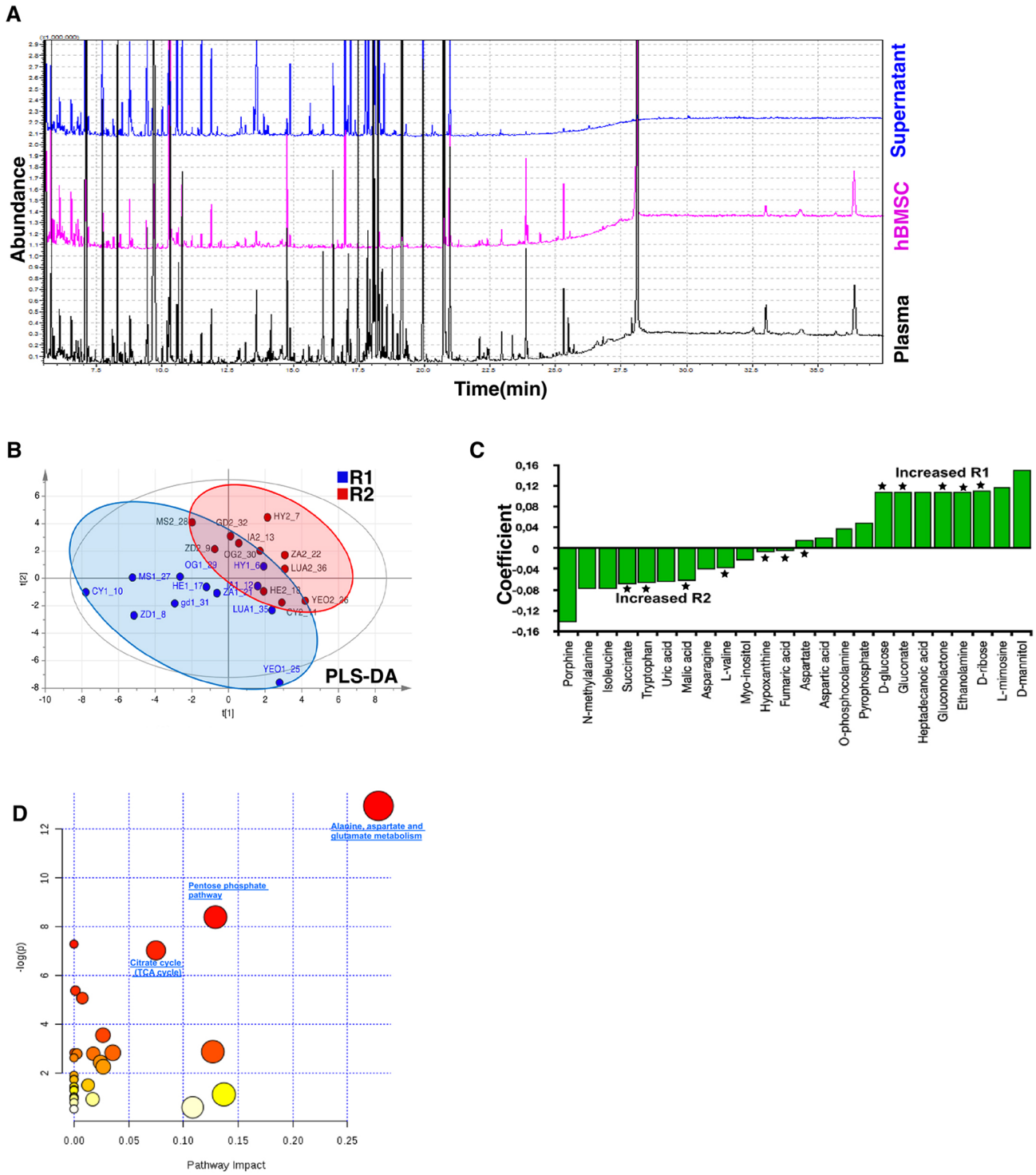

Fig. 3. According to the metabolomics analysis of plasma samples, the energy metabolism in the R1 and R2 regions is different. (A) Representative total ion chromatograms of BM plasma samples, hBMSCs and culture supernatants. (B) Multivariate analysis of data. PLS-DA loadings plot of the R1 (blue) and R2 (red) regions explaining the separation in C. (C) Regression coefficient analysis of metabolites determined via a VIP plot that highlights discriminatory metabolites. The stars indicate the metabolites with statistically significant differences between the R1 and R2 regions (Wilcoxon rank sum test, $P<0.05$). (D) Pathway analysis for metabolites that were significantly different between R1 and R2 plasma metabolomic profiles using MetaboAnalysis. Alanine, aspartate and glutamate metabolism (FDR=1.9E-4), pentose phosphate (FDR=9E-3), citrate cycle (FDR=0.01) and aminoacyl-tRNA biosynthesis (FDR=0.001) pathways are the most statistically significant pathways ($P<0.05$, FDR<0.01).

metabolites (paired *t*-tests, $P<0.05$), including D-ribose, D-glucose, gluconate and gluconolactone were identified in R1, whereas other important metabolites, including succinate, isoleucine, uric acid and malic acid, were detected in R2 (Fig. 3C). These metabolites were found to have roles in many different pathways. The alanine, aspartate and glutamate metabolism [false discovery rate

Journal of Cell Science (2021) 134, jcs250720. doi:10.1242/jcs.250720

(FDR)=1.9×10^{-4}], pentose phosphate (FDR=9×10^{-3}), citrate cycle (TCA cycle; FDR=0.01) and aminoacyl-tRNA biosynthesis (FDR=0.001) pathways were the most statistically significant (P<0.05 and FDR<0.01) (Fig. 3D). Although the pentose phosphate pathway was found to be associated with the R1 region, the citrate cycle pathway was associated with the R2 region; therefore, this result reveals that these two regions predominantly use different types of energy metabolism.

Some metabolic properties of the *in vivo* marrow microenvironment were preserved even in culture under *in vitro* normoxic conditions for weeks

Plasticity in metabolism allowing stem cells to match the divergent demands of quiescent state, self-renewal and differentiation has been the main determinant of the formation of different hematopoietic niches in the BM. In particular, differences in the dynamics and metabolic flow between energy metabolisms in different niches determines the fate of the cell populations in the marrow (Bahat and Gross, 2019; Folmes et al., 2012; Yuan et al., 2019). Because we detected a statistically significant difference between plasma samples from two regions for energy metabolism, we analyzed the metabolic flow in culture supernatants from P0 to P3 by removing MSCs from their *in vivo* environment and culturing them under *in vitro* normoxic conditions (Fig. 4).

P0 and P3 culture supernatants of hBMSCs isolated from R1 and R2 regions were analyzed with GC-MS (footprinting), and a total of 288 metabolites were determined (Fig. 4A,B). Additionally, the metabolic profiles of both the same passages of different regions (Fig. 4G–I) and the different passages of the same region (Fig. 4C–E) were analyzed comparatively, and the metabolites with the highest VIP score (Fig. 4H–J and Fig. 4D–F, respectively) were determined for each group. Metabolite profiles of P0 and P3 culture supernatants of the R1 region were analyzed comparatively and adenosine monophosphate (AMP) and tryptophane were higher in P0, whereas metabolites such as oxalic acid, creatinine, ketoleucine and urea were higher in P3 (Fig. 4C,D). Pathway analysis of these metabolites showed that these metabolites were significantly related to aminoacyl-tRNA biosynthesis (P=0.002), nitrogen metabolism (P=0.003), galactose metabolism (P=0.003), pantothenate and CoA biosynthesis (P=0.01), beta-alanine metabolism (P=0.02), arginine and proline metabolism (P=0.02), propanoate metabolism (P=0.03) and purine metabolism (P=0.03) (MetaboAnalysis, P<0.05 and FDR<0.01). Similarly, when the metabolite profiles of P0 and P3 culture supernatants of R2 were analyzed comparatively, phosphate was found to be higher in P0, whereas some metabolites, such as 1-monooctadecanoylglycerol (1-MG), ketoleucine, malic acid and succinate, were found to be higher in P3 (Fig. 4F). Pathway analysis of these metabolites were found to be significantly related to aminoacyl-tRNA biosynthesis (P=0.002), the citrate cycle (P=0.009), thiamine metabolism (P=0.013), alanine, aspartate and glutamate metabolism (P=0.013). We also analyzed the metabolite profiles of the same passages of different regions comparatively. When metabolite profiles of P0 culture supernatants of R1 and R2 were analyzed comparatively, although some metabolites, including lauric acid and palmitic acid pyridoxine, were found to be higher in R1, important metabolites, such as benzoic acid, fumaric acid and succinic acid, were found to be higher in R2 (Fig. 4H). Pathway analysis showed that these metabolites were significantly related to aminoacyl-tRNA biosynthesis (P=5×10^{-5}), phenylalanine metabolism (P=7×10^{-4}) thiamine metabolism (P=0.001), glutathione metabolism (P=0.005), arginine and proline metabolism (P=0.005), and the citrate cycle (P=0.01).

As a result of the detailed comparative analysis of metabolic profiles in culture supernatant samples, the best PLS-DA separations were detected between the P0 and P3 metabolite profiles of each region. Both at R2 P0 versus R1 P0, and after progression from P0 to P3 in each region, cells were found to enter the citrate cycle (P<0.01 and P<0.009, respectively). These results supported the notion that some *in vivo* properties of the different niches were mainly preserved even in *in vitro* culturing conditions for weeks. Culture supernatants of MSCs isolated from R1 and R2 regions still showed differences in energy metabolism, even in progressive passages (P3 versus P0).

Comparison of hBMSC metabolomic and transcriptomic data

To illuminate how region-specific metabolic profiles are in the intracellular environment and which molecular mechanisms are managing them, we examined P3-MSCs obtained from R1 and R2 regions by using metabolomic and transcriptomic analysis. GC-MS analysis of P3-hBMSCs identified 268 metabolites. Statistically significant metabolites that caused different spatial distribution in BM regions in PLS-DA analysis (Fig. 5A) were identified as o-phosphocolamine, 4-hydroxyproline and myo-inositol (Wilcoxon rank-sum test; P<0.05) (Fig. 5B,C). In the pathway analysis of these metabolites, only the sphingolipid metabolism pathway was statistically significant (pathway impact and P-value <0.05) (Fig. 5D).

At the same time, transcriptomic profiles of P3-hBMSCs from R1 and R2 regions were determined by RNA-seq and these data were analyzed (Fig. 6). As a result of RNA-Seq analysis, 26,364 genes expressed in hBMSCs of both regions were mapped. When the hBMSCs of R1 and R2 were analyzed comparatively using DESeq2, 970 differentially expressed genes (P<0.05) were identified (Fig. 6A). Of these, 468 genes were upregulated in R1 and these are associated with the cell cycle, ribosomes, the gap junction, pyrimidine metabolism, FoxO signaling and p53 signaling pathways (Fig. 6B), whereas 502 genes were found to be upregulated in R2, and these genes were associated with only the ECM-receptor interaction pathway (Fig. 6C; less than 1%, FDR <0.01). In addition, when we used q_{adj}<0.05 as the criteria for defining differentially expressed genes, 44 genes were identified and 20 out of 44 genes with a significant difference in expression were upregulated in R1, whereas 24 genes were upregulated in R2 (all gene sets are reviewed in Fig. 6D,E and Fig. S2). Although differentially expressed genes in R1 were related to cellular signaling and secretion, such as *de novo* post-translational protein folding, regulation of angiogenesis, growth factor binding, cell-substrate adhesion, transmembrane receptor protein tyrosine kinase activity, positive regulation of cell motility, positive regulation of cell migration, positive regulation of cellular component movement, positive regulation of locomotion transmembrane receptor protein kinase activity and regulation of focal adhesion assembly, differentially expressed genes in R2 were found to be related with the extracellular matrix (ECM), such as ECM organization, extracellular structure organization and keratan sulfate catabolic process (Fig. 6F,G).

What is the mechanism trying to protect energy metabolisms in MSC cultures under *in vitro* normoxic conditions?

As expected, P3-hBMSCs could not maintain region-specific energy metabolism as in their plasma by metabolomic analysis. But, interestingly, a single pathway [sphingolipid metabolism included O-phosphoethanolamine (PE) metabolite and *SPHK1* gene expression] was significantly different between the two regions according to the metabolomic and the comparative

Journal of Cell Science (2021) 134, jcs250720. doi:10.1242/jcs.250720

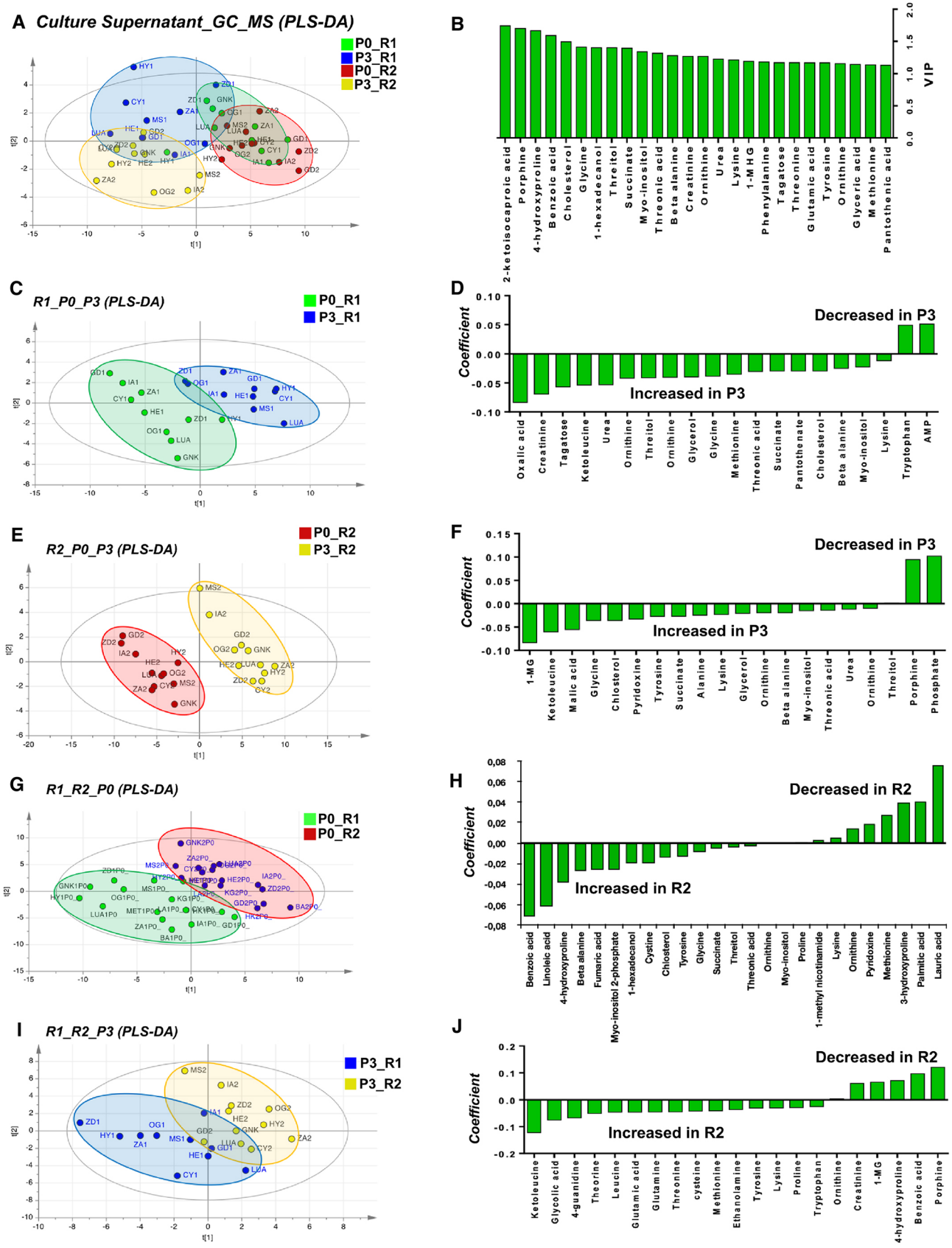

Fig. 4. See next page for legend.

Journal of Cell Science (2021) 134, jcs250720. doi:10.1242/jcs.250720

Fig. 4. Comparative metabolomic analyses of culture supernatants from the same passages of different regions and the different passages of the same region. (A) Representative multivariate analysis of all culture supernatant metabolome data. PLS-DA scores plot show the following samples: P0 of R1 region (P0-R1, green), P3 of R1 region (P3-R1, blue), P0 of R2 region (P0-R2, red), and P3 of R2 region (P3-R2, yellow). (B) Associated VIP plot highlighting the major discriminatory metabolites between culture supernatant groups. (C) PLS-DA plot of P0 (green) and P3 (blue) culture supernatants of hBMSCs isolated from the R1 region (R1-P0-P3). (D) Regression coefficient analysis of the PLS-DA plot in C. (E) PLS-DA plot of P0 (red) and P3 (yellow) culture supernatants of hBMSCs isolated from the R2 region (R2-P0-P3). (F) Regression coefficient analysis of the PLS-DA plot in E. (G) PLS-DA plot of P0 culture supernatants of hBMSCs isolated from the R1 (green) and R2 (red) region (R1-R2-P0). (H) Regression coefficient analysis of the PLS-DA plot in G. (I) PLS-DA plot of P3 culture supernatants of hBMSCs isolated from the R1 (blue) and R2 (yellow) region (R1-R2-P3). (J) Regression coefficient analysis of the PLS-DA plot in I.

metabolomic and transcriptomic analysis. There was higher *SPHK1* mRNA expression level in R1-P3-MSCs, and a high level of PE metabolite was detected in the R2-P3-MSC metabolome profile. Studies have indicated that the endosteal niche of BM is hypoxic and this hypoxic microenvironment protects stemness. *SPHK1* has been recently described as a new modulator of *HIF1A*, which is one of the major mediators of hypoxia. (Ader et al., 2008; Cho et al., 2011). Therefore, we investigated the relationship between the transcriptome profiles of two anatomically different regions with the *HIF-1* signaling pathway (Fig. 7).

When the relationship between *HIF1A*, *SPHK1* and other upregulated genes in R1 was investigated by protein-protein interaction (PPI) analysis, it was found that there is a tight relationship between these genes in R1 (Fig. 7A,B). According to these analyses, statistically significant associated pathways with these genes were FOXO signaling pathways (FDR 2e-6, including *PLK1*, *PLK2* and *CCNB1*), axon guidance (FDR 2,51e-7, including *SEMA3A*, *SEMA4B*, *EPHA2*, *EPHA3* and *NRP1*), the *HIF-1* signaling pathway (FDR 7,3e-4) and the PI3K-Akt signaling pathway (FDR 0.001).

To confirm these data, expression levels of *SPHK1* and *HIF-1* signaling pathway-associated genes (*HIF1A*, *VHL* and *PHD2*) in R1, R2 and the peripheral blood mononuclear cell (PBMC) were tested using real-time PCR analyses (Fig. 7C). *SPHK1* expression level was eightfold and 3.5-fold higher in R1 and R2, respectively,

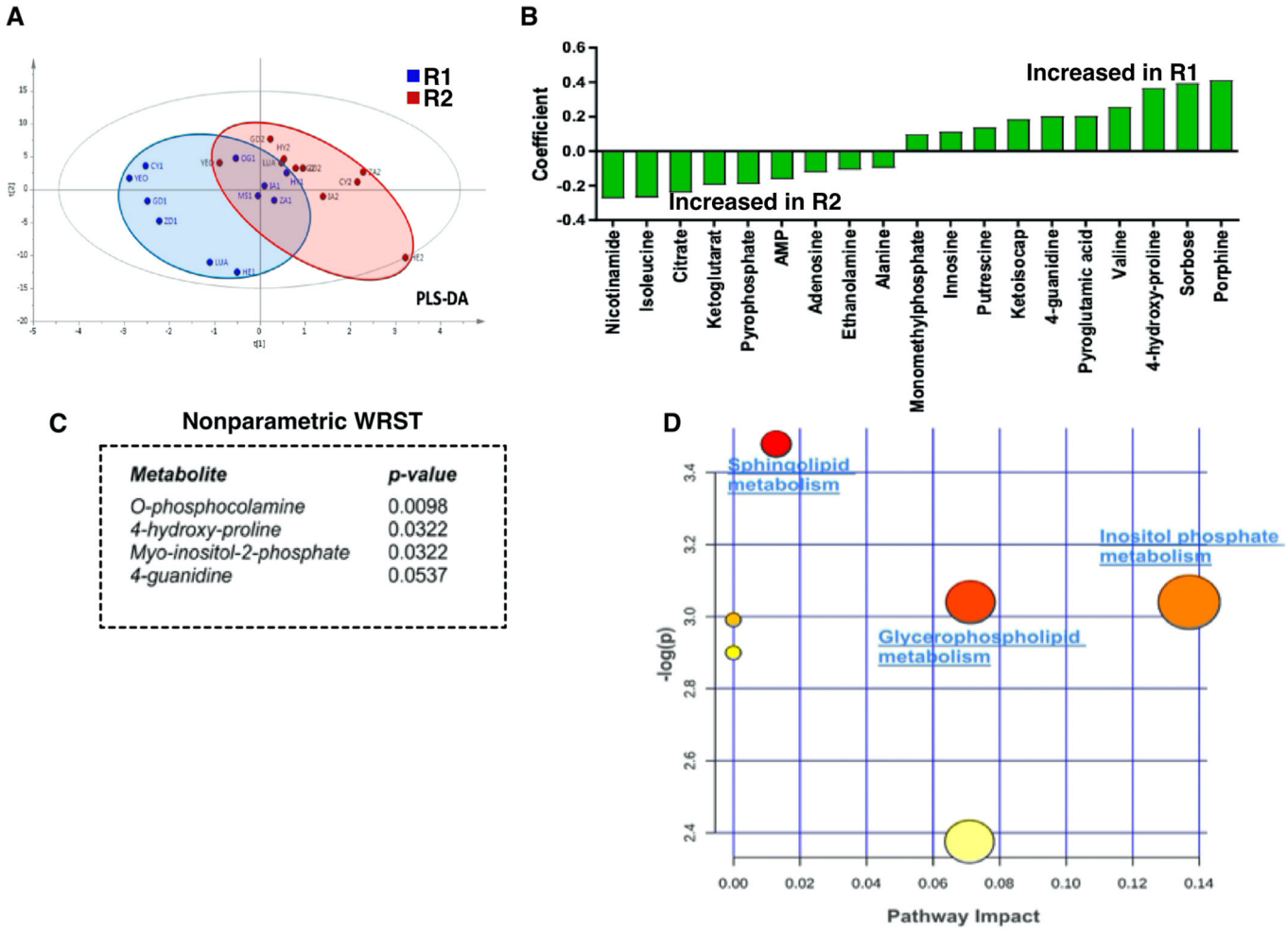

Fig. 5. Only the sphingolipid metabolism pathway is statistically significant in the metabolomics multivariate analysis of the hBMSCs of two regions. (A) Representative multivariate analysis of hBMSCs. PLS-DA scores plot shows cell samples from the R1 region (blue) and R2 region (red). (B) Regression coefficient analysis highlighting discriminatory metabolites determined via the VIP plot. (C) O-phosphocolamine (also known as O-phosphoethanolamine), 4-hydroxyproline and myo-inositol are statistically significant metabolites that caused the different spatial distribution of BM regions in the PLS-DA analysis in A (P<0.05). (D) Pathway analysis of the significantly different metabolites shown in C. Only the sphingolipid metabolism pathway is statistically significant (pathway impact and P<0.05).

Journal of Cell Science (2021) 134, jcs250720. doi:10.1242/jcs.250720

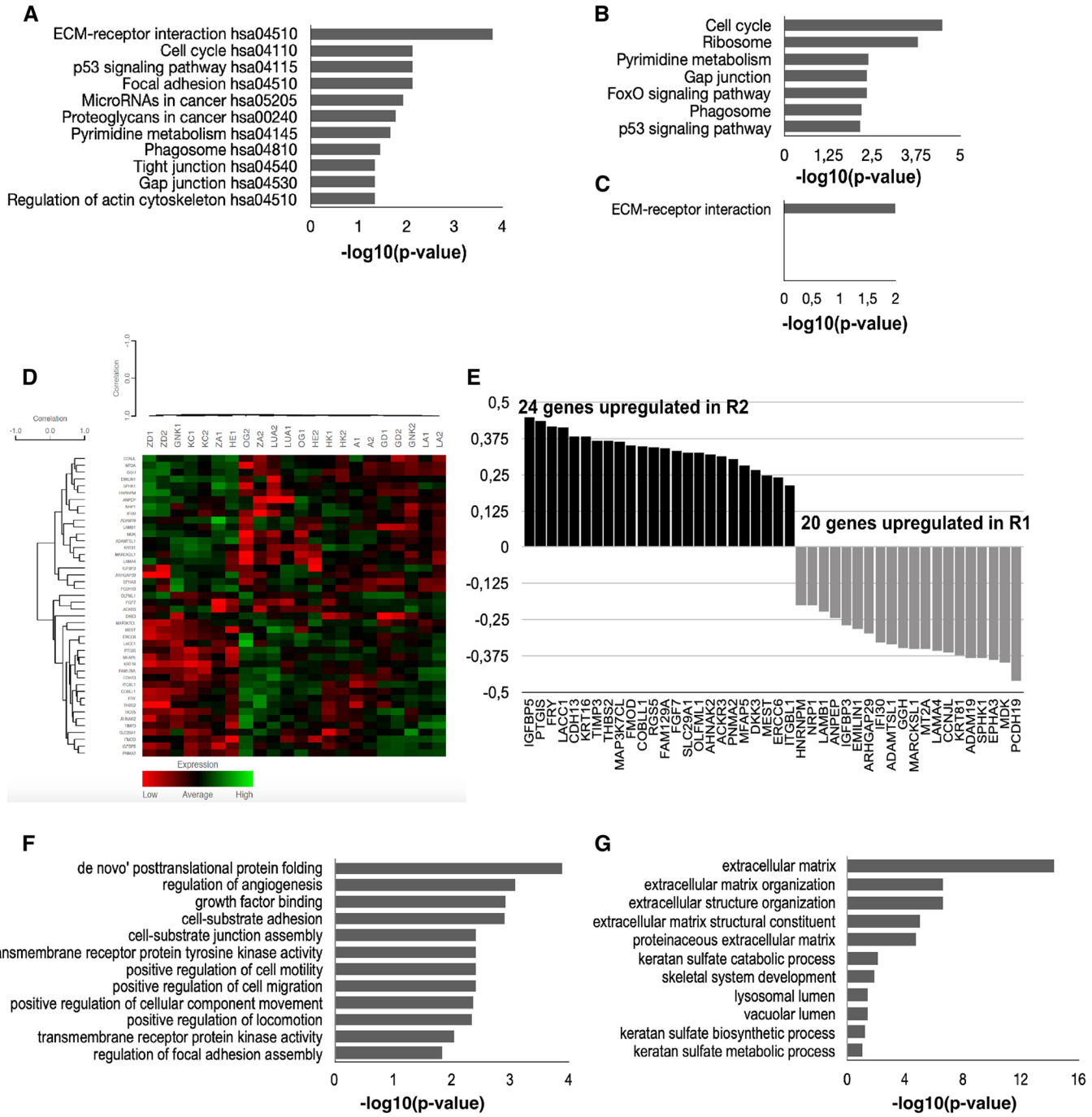

Fig. 6. Transcriptome data analyses of P3-hBMSCs from the R1 and R2 regions. (A) Enriched KEGG analysis, based on a total of 970 differentially expressed genes detected via DESeq2 analysis [using $P<0.05$ in DESeq2, less than 1% FDR (<0.01) and $P<0.05$ in the KEGG pathway analysis as the criteria]. (B) Enriched KEGG analysis, based on 468 genes upregulated at R1 from 970 genes in A [using $P<0.05$ in DESeq2, less than 1% FDR (<0.01) and $P<0.05$ in the KEGG pathway analysis as the criteria]. (C) Enriched KEGG analysis based on 502 genes upregulated at R2 from 970 genes in A [using $P<0.05$ in DESeq2, less than 1% FDR (<0.01) and $P<0.05$ in the KEGG pathway analysis as the criteria]. (D) Heatmap showing 44 differentially expressed genes ($q_{adj}<0.05$), high (green) or low (red) expression, between R1 and R2 regions of each donors ($n=11$) (a more detailed and readable view of heatmap alignments are given in Fig. S2). (E) Representative distributions and fold changes in the regions of 44 differentially expressed genes (DEG) (*x*-axis, 44 DEG set; *y*-axis, fold change). (F,G) Top enriched GO terms of 20 genes upregulated in R1 (F) and 24 genes upregulated in R2 (G).

compared to PBMC (PBMC was used as negative control). There was no significant difference in *HIF1A* and *VHL* gene expression between regions, although *HIF1A* expression decreased threefold and *VHL* expression increased 11-fold in the PBMC. *PHD2* (also known as *EGLN1*) gene expression was the same in the PBMC and R2, although it increased ∼twofold in R1.

DISCUSSION

Though the presence of different HSC niches in the BM has been demonstrated through several model organisms and experimental models (Abarrategi et al., 2018; Ellis and Nilsson, 2012; Lo Celso et al., 2009), these niches have been difficult to characterize, especially in healthy people, as access to healthy human BM

Journal of Cell Science (2021) 134, jcs250720. doi:10.1242/jcs.250720

samples for research is very limited. The healthy human BM samples are usually obtained from BM transplant donors through random aspirations during BM harvest for transplantation. To date, studies on the microenvironments of HSCs have not addressed an optimal BM sample collection method from different BM niches. With this goal in mind, only detailed studies on samples obtained by superficial and deep aspirations may reveal different profiles that may suggest the presence of functionally distinct niches. This aspect of the study presents an original comparative analysis (transcriptomic and metabolomic) pertaining to the characterization of two different anatomical BM regions (superficial and deep aspirations) of healthy humans.

The results of our analyses have shed light on two important issues. First, we obtained BM samples from anatomically very close regions to each other of the same tissue of the same individual, and achieved high similarity in terms of gene expression and metabolite profiles among both regions and individuals. This detailed human BM characterization may help better understanding of stem cell biology, creating an important opportunity for further research on hematological disorders, cancer, BM transplantation (BMT) fields and regenerative medicine. Second, we detected statistically significant differences between the two regions in both metabolomic and transcriptomic findings. These results suggested the presence of functionally distinct niches in the human BM. Considering the paucity of stem cell niche studies on human samples, the omics data presented here may contribute to the delineation of the BM niche physiology according to anatomical location, thus it may also lead to the consideration of more efficient techniques of BM harvest.

Until today, in the BM niche studies, although different techniques, such as enzymatic or mechanic isolation or three-dimensional imaging, have been used to distinguish niches, the common opinion in all of these studies is that most of both the HSCs and the stromal cells are concentrated in the endosteal niche (Cordeiro Spinetti et al., 2015; Ehninger and Trumpp, 2011; Guezguez et al., 2013; Mendelson and Frenette, 2014; Muschler et al., 1997; Patterson et al., 2017; Sugiyama et al., 2006). In this study, we used BM aspiration at a volume of 3 ml from both regions, R1 and R2, to represent endosteal (osteoblastic) and vascular (perisinusoidal) regions, respectively (Fig. S1). The first point that attracted our attention was that the number of total MNCs isolated from R1 was higher than R2 after Ficoll gradient isolation (Fig. 1A; Table S1). R1-P0-hBMSCs showed higher adhesion and proliferation than the R2-P0-hBMSCs after seeding the MNCs, but this difference disappeared as passages progressed in *in vitro* culture conditions (Fig. 1C). These findings show that as MNCs contain a heterogeneous group of non-hematopoietic cells, R1-MNCs contain more stem and progenitor cells than R2-MNC. In other words, R1-MNCs begin attachment and colony forming with more MSCs. However, the disappearance of this difference between regions through progressed passage may be explained by P3-BMSCs from both regions having a more homogeneous cell population in *in vitro* culture conditions in which *in vivo* microenvironment conditions disappeared. Therefore, this data may show that the two regions have different *in vivo* microenvironment conditions, and our superficial and deep aspiration technique may suggest the presence of functionally distinct niches. The ability to differentiate into cell types different from the tissue of origin has been termed adult stem cell plasticity, and recently, most of the metabolomic studies have been focused on the discovery of metabolites that retain the plasticity of the stem cells or encourage them to differentiate (Folmes et al., 2012). In particular, plasticity in energy metabolism that determines stem cell fate (self-renewal or differentiation) has been the main determinant of the formation of different hematopoietic niches in the BM (Bahat and Gross, 2019). Moreover, the metabolic flow between energy metabolisms in niches determines the fate of cell populations in the marrow. Numerous studies have shown that oxygen concentration in BM gradually increases from the endosteum to sinusoids. At a low oxygen environment, also known as hypoxia, in the endosteal niche of BM, cells maintain quiescence as a mechanism to maintain their self-renewal capacity, to protect from the accumulation of cellular damage caused by stress and to provide tissue regeneration throughout the lifetime. In quiescent status, cells have high colony-forming capacity, low NADH and low mitochondrial membrane potential, and the cells prefer to use the anaerobic glycolysis and pentose phosphate pathways to meet their anabolic requirements for replication (amino acid, nucleotide, sugar, etc.) instead of mitochondrial respiration with high energy. Hypoxia and regulation of hypoxia-inducible factor 1α (HIF1A), a marker of hypoxia, induces the increasing activity of enzymes and glucose transporters involved in the glycolytic pathway. Conversely, in the vascular niche of BM, cofactor (NADPH) and energy (ATP) consumption significantly increase during proliferation and differentiation, and the cells enter the oxygen-dependent mitochondrial tricarboxylic acid (TCA) cycle (Folmes et al., 2012; Guarnerio et al., 2014; Ochocki and Simon, 2013; Szade et al., 2018). Metabolomic data obtained from plasma samples, which may be better representative of the *in vivo* BM microenvironment, has suggested that there was a significant difference in energy metabolism between R1 and R2 regions. The metabolites associated with pentose phosphate and glycolysis pathways were found in R1, whereas the metabolites associated with the TCA cycle were found in R2 (Fig. 3).

However, R1- and R2-derived culture supernatants of MSCs from later passages (P3 versus P0) continue to exhibit differences in energy metabolism. These data support the notion that *in vivo* properties are preserved even if these cells are cultured for weeks under *in vitro* normoxic conditions (Fig. 4). In the detailed comparative analysis of culture supernatant metabolic profiles of both the same passages of different regions and the different passages of the same region, the best PLS-DA separations were detected between the P0 and P3 metabolite profiles of each region. In the R2 region versus R1 at P0 (Fig. 4G) and during the progression from P0 to P3 in the R2 region (Fig. 4E), cells entered the citrate cycle ($P<0.01$). These results support the notion that R1 and R2 regions differ from each other in energy metabolism.

Interestingly, there was no significant difference in energy metabolisms between the P0 and P3 metabolite profiles of the R1 region. Therefore, we hypothesized that another hypoxia regulatory mechanism other than low oxygen level may be active in the R1 region as the MSCs were cultured under normoxic conditions in this study. Our comparative metabolomic and transcriptomic analyses revealed the significant involvement of sphingolipid metabolism (included PE and *SPHK1* mRNA). *SPHK1* mRNA expression was increased in R1-P3-MSCs (Fig. 6E), and high PE expression was detected in the R2-P3-MSC metabolome profile (Fig. 5C). In previous studies, *SPHK1* has been defined as a new modulator of *HIF1A* in hypoxia (Ader et al., 2008; Cho et al., 2011). Low oxygen conditions stimulate *SPHK1* activity and this activity is regulated by ROS (Ader et al., 2008). The SPHK1 protein catalyzes the phosphorylation of sphingosine and then sphingosine-1-phosphate (S1P) is formed. Phosphorylation of sphingosine changes its catalytic activity and induces its translocation from the cytosol to the plasma membrane. Many studies have shown that S1P plays an important role in many biological processes of stem cells, from self-renewal to differentiation. On the other hand, when S1P is

Journal of Cell Science (2021) 134, jcs250720. doi:10.1242/jcs.250720

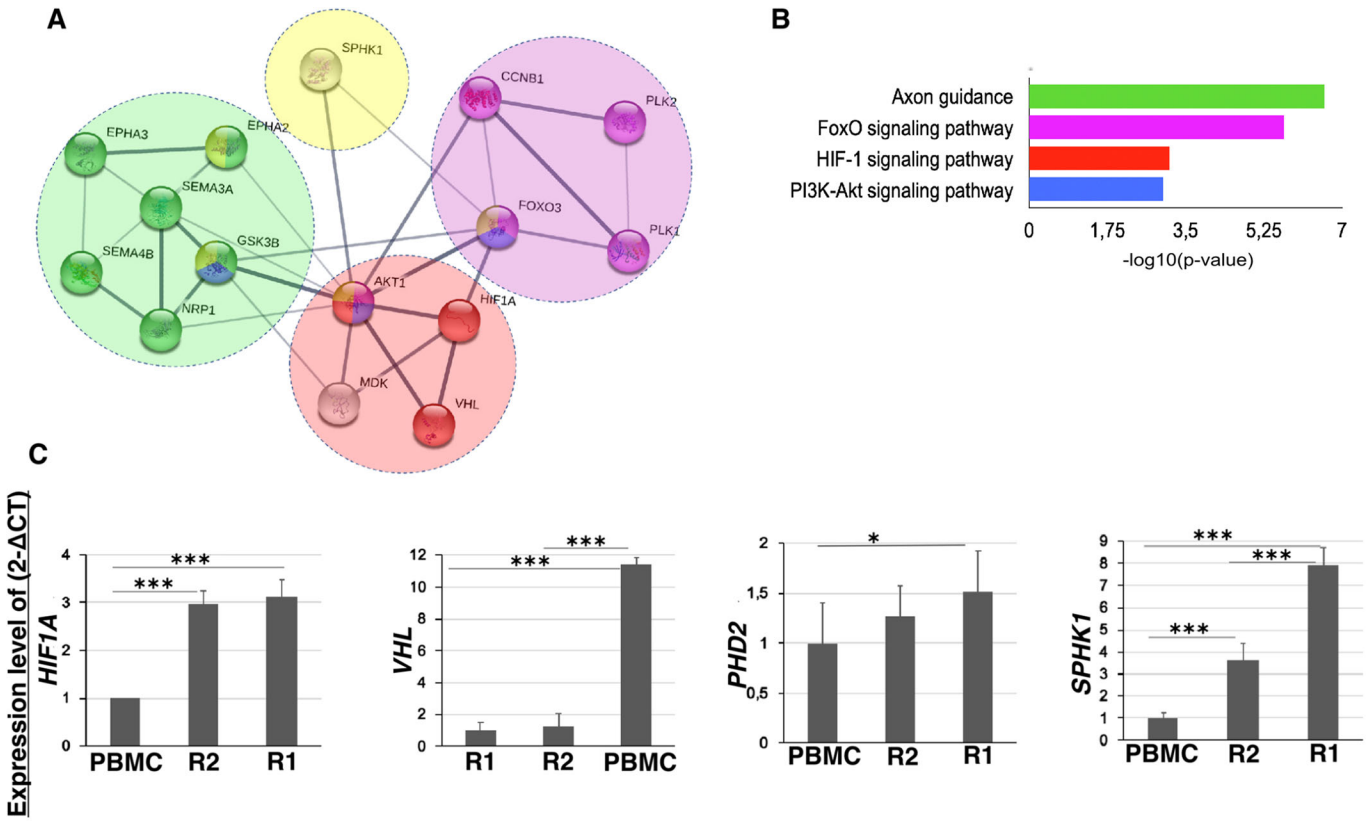

Fig. 7. The relationship between transcriptome profiles of two anatomically different regions with the HIF1 signaling pathway. (A) PPI analysis of the relationship between *HIF1A*, *SPHK1* and other upregulated genes in R1. The purple gene cluster consists of upregulated genes associated with FOXO signaling pathways detected in the R1 region. The green gene cluster consists of upregulated genes associated with axon guidance signaling pathways detected in the R1 region. The yellow cluster consists of the upregulated *SPHK1* gene in the R1 region. The red gene cluster consists of HIF-1 signaling pathway genes found to be associated with these genes in R1. (B) *P*-value chart of associated pathways in A. (C) The relative expression levels of the *SPHK1* and *HIF-1* signaling pathway-associated genes (*HIF1A*, *VHL* and *PHD2*) based on the qPCR measurements of R1, R2 and PBMC. Data are mean±s.d. **P*<0.05, ****P*<0.001 (two-tailed, paired *t*-test).

irreversibly cleaved by S1P lyase, it is degraded into hexadecenal and O-phosphoethanolamine (Lidgerwood et al., 2018). Our analyses suggested that there is S1P activation in R1 but degradation in the R2 region of the BM. *SPHK1* suppresses active *VHL* and shows activation by inhibition of the degradation instead of increasing the expression of *HIF1A*. Accumulated *HIF1A* promotes the expression of glycolytic metabolism-related genes. Expression of these genes enables metabolism flux from oxidative phosphorylation to glycolysis and subsequently maintains stemness and self-renewal while inhibiting differentiation, ROS generation and apoptosis. Furthermore, real-time PCR (Fig. 7C) analysis showed the *SPHK1* gene has eightfold and 3.5-fold higher expression level in R1 and R2, respectively, compared to PBMC. There was no significant difference in *HIF* and *VHL* gene expression between regions, whereas *HIF1A* expression decreased threefold and *VHL* expression increased 11-fold in PBMC. Additionally, *PHD2* expression was the same in PBMC and R1, whereas it increased ∼twofold in R2.

As a result of our transcriptomic analysis, in addition to *SPHK1*, genes related to the *FOXO* signaling pathway, which is important in energy metabolism, and the axon guidance pathway were found to be statistically significant and upregulated in the R1 region versus R2. Also, we showed that there is a tight relationship between the *HIF-1* signaling pathway and these pathways in R1 (Fig. 7A,B). *Sema3A* defined in the axon guidance pathway and bone biology plays an important role in canonical Wnt/β-catenin signaling (Li et al., 2017). As has been well established, canonical Wnt/β-catenin signaling is one of a number of specific BM osteoblastic niche mechanisms that regulate the unique stem cell features (such as their self-renewal, quiescence state and multipotentiality) (Ahmadzadeh et al., 2016; Sugimura et al., 2012). Many other studies have shown that *NRP1* is upregulated by Wnt signaling in stem cells (Suda and Arai, 2008). Binding of *SEMA3A* to *NRP1* with high affinity is a special signaling pathway. Mutant Sema3a and Nrp1 mice studies have shown that osteoblast number decreased, bone formation rate reduced and adipocyte number increased. In addition, *NRP1* serves as a co-receptor for *SEMA3A*, and dominant *SEMA3A* has a negative effect on *VEGFA* and increases proliferation of $CD34^{+}$ cells through competition for the *NRP1* receptor (Palodetto et al., 2017). Moreover, *SEMA3A* controls *NRP1*-mediated forkhead box O (*FOXO*) 3 activation. *FOXO3* is one of the major genes in the *FOXO* signaling pathway. FOXO3 both inhibits ROS production through ROS detoxification and activates HIF1A through inhibition of PHDs under hypoxia (Peck et al., 2013). In contrast to the R1 region in which *NRP1* and *SEMA3A* were upregulated, we found that Dickkopf WNT signaling pathway inhibitor 3 (*DKK3*) was upregulated in the R2 region (Fig. 6E). Recombinant *DKK3* protein studies indicated that exogenous *DKK3* protein inhibits Wnt/β-catenin signaling (Xu et al., 2017). These results support the notion that R1 and R2 regions differ from each other in quiescence and osteoblastic activity.

Moreover, transcriptome analysis of this study on P3-MSCs revealed that there was a high expression level of the *ACKR3* (herein

Journal of Cell Science (2021) 134, jcs250720. doi:10.1242/jcs.250720

referred to as *CXCR7*) gene in R2 versus R1, whereas there was no difference in *CXCL12* expression (Fig. 6E). *CXCR7* and *CXCR4* are chemokine receptors for *CXCL12* and they play an essential role in hematopoietic cell migration and homing induced by *CXCL12*. The CXCL12-CXCR4 complex plays an important role in maintaining the quiescent state of HSCs, whereas the CXCR7-CXCL12 complex is a negative regulator of CXCL12. Downregulation of *CXCL12* through *CXCR7* allows the cycle of HSCs and their mobilization to peripheral blood from the endosteal niche (Ahmadzadeh et al., 2015; Asri et al., 2016). *CXCR7* also has a regulatory role in the function of the *CXCL12/CXCR4* signaling pathway. *CXCR7* deficiency results in increased *CXCL12* protein levels, whereas *CXCL12* mRNA levels are unchanged (Koenen et al., 2019; Sánchez-Alcañiz et al., 2011). Similarly, in our analysis, there was no difference in *CXCL12* mRNA levels between regions, whereas *CXCR7* was significantly upregulated in R2. These data support the notion that the R1 region close to the bone plays a role in the maintenance of the quiescent state of the HSC pools, whereas the R2 region promotes HSC mobilization.

All biological processes (including growth, differentiation, motility and viability) of HSCs are regulated by interactions with the ECM of the BM via integrins (such as CD29) and adhesion molecules (such as CD44). The ECM of the BM, which acts as storage for growth factors and cytokines, consists of cytokine-binding glycosaminoglycans, FN, laminin, collagen types I and IV, hyaluronan, heparin sulfate and chondroitin sulfate (Krause et al., 2013). *CXCR4* and *CXCR7* regulate the interactions between hyaluronic acid (HA) receptor CD44, ligand HA and CXCL12, and eventually provide the balance between endosteal homing and endothelial migration of hematopoietic stem and progenitor cells within specific niches of the BM. The interaction between the stromal cell receptor CD44 and the ligand HA synthesized by HSCs is stimulated by CXCL12 (Avigdor et al., 2004; Tamma and Ribatti, 2017). Although flow cytometry results of R1 and R2 regions were similar, according to our immunofluorescence staining results, the hyaluronate receptor CD44, CD29, osteopontin (OPN) and fibronectin (FN) had higher fluorescent intensity in the R1 region close to the bone sites of marrow versus R2 (Fig. 2). Similarly, osteopontin (OPN), which is secreted by osteoblast progenitors (OPs), osteoblasts and MSCs in bone sites, plays an important role in attracting HSCs toward the endosteal region and maintaining the their quiescent state. This process involves CD29, which regulates the homing of hematopoietic progenitors to the BM (Krause et al., 2013; Tamma and Ribatti, 2017). CD29 expression was much stronger in R1 compared to R2 (Fig. 2B). All of these findings suggest that the R1 region may represent the endosteal niche.

In conclusion, this study suggests that limiting aspiration volume to 3 ml per needle position during BM harvest and the collection of BM samples from superficial and deeper sites in the iliac crest may be a useful technique for studying human BM niches, and the technique may have clinical translation potential. The experimental findings of metabolomics and transcriptomics in our study provides collateral evidence for the theoretical knowledge about the hematopoietic niche, and it also supports the results of previous studies obtained in animal BM niche studies. The samples obtained by superficial aspiration in BM region R1, exhibited the main characteristics of the endosteal niche, whereas the deeper BM region R2 exhibited the characteristics of the vascular niche. The determination of detailed metabolic and transcriptomic profiles of healthy human BM microenvironment and BMSCs is valuable and has implications in regenerative medicine in terms of (1) the determination of the optimum requirements for the cells in *in vitro* culture media, (2) the design of the appropriate microenvironment for *in vitro* HSC niche modelling, which is still quite difficult, or (3) providing the reference values that can be compared in disease states, including hematologic malignancy, BM failure syndromes.

MATERIALS AND METHODS

Experimental model and subject details

BM aspiration samples were obtained from 11 healthy donors of patients who received BMT at the BMT Unit of İhsan Doğramacı Children's Hospital at Hacettepe University. This study was conducted according to the principles expressed in the Declaration of Helsinki. Ethical approval of this study was obtained from the Hacettepe University Non-invasive Clinical Research Ethics Committee (GO 13/172) (donor information is provided in Table S1). Informed consent forms were signed and all experiments were performed in accordance with the approved guidelines and regulations.

In 'standard BM harvest practice', transplant physicians perform multiple superficial and deep aspirations from the iliac crest of donors using an aspiration needle, which is inserted at diverging angles at the same points and moved back and forth. The same process is repeated at several different points until a sufficient marrow sample is obtained. Although the size and bone mass of the donors is variable, samples obtained by experienced physicians from the superficial region are expected to be highly representative of the marrow area close to the bone cortex. Similarly, a deeper BM sample in experienced hands will represent an area distant from the bone cortex. It is not clear whether the deeper region is the central marrow or vascular region, but it is evidently away from the bone cortex (Friedlis and Centeno, 2016; Hernigou et al., 2014; Lee et al., 2008; Shapiro and Arthurs, 2017).

Unlike the standard practice, BM samples used in the 'present study' were obtained from 'two different anatomic regions' of the healthy BM donors. A similar 'two different anatomic regions' technique had been performed by Muschler in 1997 (Muschler et al., 1997) and Patterson in 2017 (Patterson et al., 2017) to obtain OPs from the human iliac crest. These studies recommended small volumes (about 2 ml) of aspiration to counteract the risk of dilution of the BM sample with sinusoidal blood during BM aspiration from the deeper marrow site. Under the guidance of these previously published studies, our BM samples were named as 'R1' whereby one-time aspiration samples were obtained right after the aspiration needle passed the bone cortex and entered the marrow space. Then the aspiration needle was pushed forward towards the center of the BM and one-time aspiration samples were taken from the deeper marrow site and named as 'R2'. As a standard, the aspirated BM samples from each region of all donors were limited to 3 ml. All aspirations were made by the same experienced transplant physician. A model illustrating HSC niches and needle localizations during BM aspiration according to our BM harvest in Fig. 1.

Collection of plasma and preparation of hBMSC

The MSCs isolated from the marrow aspirated from R1 and R2 regions were named R1-hBMSC and R2-hBMSC, respectively. For the MSC isolation, 3 ml heparinized BM samples were transferred into 15 ml conical centrifuge tubes and centrifuged at 453 ***g*** for 5 min. Plasma samples were collected and divided into aliquots of 100 µl and stored at −80°C for metabolomic analysis. Plasma-free bone marrow samples were diluted with 1× Dulbecco's PBS (Gibco, Invitrogen) at a 1:1 ratio. Next, 3 ml of Ficoll-Paque Plus solution (density 1.077 g/cm^3) was placed into a 15 ml conical tube and 6 ml of the diluted BM was carefully added. The tubes were then centrifuged at 400 ***g*** without the brake for 30 min at room temperature. The white ring of MNCs, which is located between the two phases, was collected and counted (using an automated complete blood count analysis test). Then equal numbers of MNCs from each niche (10×10^6 MNCs) were seeded in a cell culture flask in Dulbecco's modified Eagle's medium (DMEM)-1×GlutaMAX (Gibco, Invitrogen) supplemented with 10% FCS (Gibco Invitrogen) and 1% penicillin/streptomycin (Invitrogen), and incubated at 37°C in a humidified 5% CO_2 atmosphere. The culture medium was completely changed twice a week. When 80% confluence was reached, adherent cells were trypsinized (trypsin-EDTA, Gibco, Invitrogen) and replated for culture expansion. Cell counts were performed with each passage and equal numbers of MSCs from each marrow region (R1-MSC

and R2-MSC) were replated at the end of each passage. P3 MSCs were used in the subsequent experiments, MSC characterization and transcriptome and metabolomic analysis.

Collection of MSCs and culture supernatants for metabolomic analysis

At the end of P0 and P3 MSC culture, on reaching 80% confluence, culture supernatants were collected and centrifuged at 300 ***g*** for 10 min. Then supernatants were filtrated through filters with a 0.45 µm pore size, divided into aliquots of 300 µl and stored at −20°C. Additionally, adherent cells were trypsinized and counted, and then 1×10^6 P3-hBMSCs in 100 µl 1× PBS were stored at −80°C for metabolic analysis.

Characterization of hBMSC by flow cytometry

Flow cytometry was performed to characterize the immunophenotypic profile of MSCs and comparatively analyze R1-hBMSCs and R2-hBMSCs. Events were acquired using a FACS ARIA cell sorter (BD Biosciences) and analyzed using FACS DIVA v8.0.1 software. To stain hMSCs, the cells were harvested and then washed with PBS. The cells were incubated for 30 min with fluorescein-labeled (FITC, PE, PerCP and APC) anti-human CD14, CD29, CD31, CD34, CD44, CD45, CD73, CD90, CD106, CD166, HLA-DR and HLA-ABC monoclonal antibodies. Incubations were done with 5 µl of each antibody in the presence of 100 µl PBN (PBS supplemented with 0.5% BSA and 0.05% NaN_3) at 2×10^4 cells per experimental tube in the dark. For control cells, FITC, APC and PE isotype control antibodies were prepared (all reagents and antibodies were acquired from eBiosciences or BioLegend, and clone, catolog and RRID numbers for all antibodies and reagents are listed in Table S2).

Characterization of hBMSC by immunofluorescence staining

To identify R1 and R2 hBMSC characteristics, P2-hBMSCs were seeded on poly-l-lysine-coated eight-well chamber slides (BD Biosciences) and cultured for 2 days. At the end of the culture, samples were rinsed in PBS and fixed in cold methanol for 10 min. Cells were incubated with 10% normal blocking serum in PBS for 30 min at 37°C. Then, cells were incubated overnight at 4°C with the CD29, CD44, FN and OPN primary antibodies (1:50 dilution). After washing with PBS (three times for 5 min each), cells were incubated with FITC-labeled appropriate secondary antibodies for 30 min in the dark. After washing with PBS and drying completely, cells were mounted with mounting medium containing DAPI (Karaoz et al., 2009). Images were acquired using a JuLI Stage-Real-Time Automated Cell Imaging System (NanoEnTek, Guro-gu, Seoul, Korea).

Characterization of hBMSC by *in vitro* adipogenic and osteogenic differentiation

P2-hBMSCs (3000 cells/cm^2) were seeded in six-well plates to induce adipogenic and osteogenic differentiation. For osteogenic and adipogenic capacity, MSCs were cultured in osteogenic medium [DMEM-1×GlutaMAX supplemented with 10% fetal bovine serum (FBS), 10 mM β-glycerophosphate, 0.1 µM dexamethasone and 50 µM ascorbic acid] and in adipogenic medium [DMEM-1×GlutaMAX supplemented with 10% FBS, 0.5 mM isobutyl-methylxanthine (IBMX), 0.1 µM dexamethasone, 10 µg/ml insulin and 0.2 µM indomethacin] for 21 days. The media were replaced twice a week. After 21 days, the osteogenic and adipogenic differentiation potential of the cells was determined by staining with Alizarin Red S and Oil-Red-O, which are indicators of osteogenic and adipogenic differentiation, respectively (Karaoz et al., 2009). The controls were cultured in the normal medium during differentiation and the medium was changed twice a week.

Transcriptomic analysis

To identify differentially expressed genes instead of heterogeneous cell populations, such as MNCs and early passage hBMSCs, only P3-BMSCs, which are generally considered to be homogeneous cell populations obtained from both regions, were analyzed comparatively by global transcriptome analysis. RNA-seq-based transcriptomic analyses were performed using an Illumina HiSeq2000 at the University of Wisconsin Biotechnology Center Gene Expression Center.

Library preparation for RNA-seq

P3-hBMSCs (1×10^6) isolated from R1 and R2 regions were stored in 1.5 ml tubes with 500 µl RNAprotect Cell Reagent (Qiagen, 76526). RNAs were extracted from hBMSCs using a Qiagen RNeasy Plus Mini kit (Qiagen, 74134) following the manufacturer's recommended procedures. The quality of all RNA samples was confirmed using an Agilent Technologies 2100 Bioanalyzer, with an RNA integrity number greater than nine recorded for all samples.

RNA (∼1 µg) was converted to double-stranded cDNA using poly-A beads to enrich for mRNA, and a TruSeq RNA Sample Preparation kit v2 (Illumina, 14669400) was used to generate strand-specific libraries. In the analyses, the DNF-473-33-SS NGS Fragment 1-6000 bp method was applied. Adapters were ligated to facilitate 3-plex sequencing on an Illumina HiSeq2000, aiming for 50 bp reads per library.

Data analysis for RNA-seq

Illumina Casava1.8.2 software was used for basecalling. Quality controls of the RNA-seq raw readings (provided information about the quality, quality score, length, GC-content of each sequence and the presence of adapters) were evaluated with Babraham Bioinformatics FASTQC software (version 0.11.2). These analyses showed that high quality sequences were obtained from all individuals, and all groups were included in the subsequent analyses.

RNA-seq reads of filtered R1- and R2-P3-MSCs were aligned to the *Homo sapiens* UCSC hg19 reference genome assembly using RNA-Seq Alignment (version 1.1.0., Illumina). The gene counts, gene FPKMs, principal component analysis and a control-vs-comparison (R1-vs-R2 regions) containing differential expression results were produced by DESeq2 (version 1.1.0., BaseSpace Labs). A subset of condition-specific expression was defined as showing a P and P-adj<0.05 in expression between R1 and R2 samples. Webgestalt GSAT, DAVID, STRING and GeneMANIA analysis software were used to analyze whether the proteins associated to differentially expressed genes that take part in a specific signaling pathway.

Validation of differentially expressed genes via qRT-PCR

The qRT-PCR SYBR Green method was used for the validation of both differentially expressed genes in R1 and R2-P3-hBMSCs, and their close interacted genes on the same pathways using an Agilent Technologies Stratagene Mx3005P Biosystems (the sequences of oligonucleotides for selected genes are included in Table S2). Peripheral blood was used as a control group. Total RNA was isolated from R1- and R2-P3-hBMSCs, and peripheral blood of all donors using a Qiagen RNeasy Plus Mini kit according to the manufacturer's instructions. Reverse transcription was performed using the QuantiTect Reverse Transcription Kit (Qiagen, 205313) following the manufacturer's recommendations. The qRT-PCR was set up using a 1 µl first-strand cDNA template, 10 µl 1× SYBR Green I master mix with ROX (Thermo Fisher Scientific, Cat K0223, Lot 00188384) as a reference dye, 0.3 mM forward and reverse gene-specific primers and 8.4 ml deionized H_2O. Then the 96-well plate was run on the qPCR machine for 40 cycles. The thermal cycling conditions were 3 min at 95°C followed by 40 cycles of 30 s at 95°C and 1 min at 60°C. The relative expression of each mRNA was analyzed using a comparative CT($2^{-\Delta\Delta CT}$) method. Fold changes were calculated as the difference in gene expression between R1 and R2 MSCs relative to peripheral blood.

Metabolomic analysis

GC-MS-based metabolomic analyses were performed as described in our previous studies (Nemutlu et al., 2015). In this study, 100 µl plasma and 1×10^6 hBMSC in 100 µl PBS samples were stored at −80°C and P0-P3 culture supernatants were stored at −20°C. All the samples were thawed on ice, and 900 µl of cold methanol:water (8:1, v/v), including 1 µg/ml myristic acid-d27 as an internal standard, was added to the samples, then vortexed for 30 s, followed by 10 min centrifugation at 14,000 ***g*** (4°C). The resultant supernatants were transferred to new tubes and were evaporated until dry at room temperature. After the solutions in the samples were completely evaporated, derivatization process with N-methyl-N-(trimethylsilyl)-trifluoroacetamide (MSTFA) plus 1% trimethylchlorosilane (TMCS) was

started. After reaching room temperature, the samples were incubated for 90 min at 30°C with 20 µl methoxamine hydrochloride/pyridine solution (20 mg/ml) for the methoximation reaction. At the end of the period, samples were expected to reach room temperature and were incubated for 30 min at 37°C after the addition of 50 µl MSTFA for the silylation reaction. At the end of the reaction, 50 µl of the reaction mixture was transferred to the GC-MS instrument for analysis.

GC-MS analysis was carried out using a Shimadzu GC-MS-QP2010 mass spectrometer. Helium (1 ml/min) was used as the carrier gas with an ultra split/splitless injector. The GC column was an Agilent 122-5532G DB5-MS column (30 m long, 0.25 mm i.d., 0.25 mm film thickness and 95% dimethyl/5% dimethyl polyethoxane). GC oven temperature programming was as follows: 1 min at 60°C, increased by 10°C per minute to 325°C and after 10 min at this temperature the oven was cooled to 60°C. The total operating time of the device is 37.5 min. Mass analyses were carried out in scan mode. MS parameters for scanning mode were as follows: mass selective detector transfer line temperature was 290°C, electron impact ionization was 70 eV, filament temperature was 230°C, quadrupol temperature was 150°C, scanning range was 50-600 Da and 2 spectra/s, and solvent delay time in the analysis was 5.90 min.

GC-MS-based metabolomic analysis was performed as described in our previous study (Nemutlu et al., 2015). The data deconvolution was conducted using AMDIS, and then SpectConnect was used to create a data matrix of metabolite peaks. Data matrices obtained from GC-MS were transferred separately to the excel files and normalized using internal standards. Subsequently, the data matrices were transferred to the SIMCA-P+ program (v13.0, Umetrics, Umea, Sweden) for multivariate analyses, such as principal component analysis and partial least squares differentiation analysis (PLS-DA) for the assessment of separability of the groups. The VIP values estimated to distinguish the most important metabolites for the separation of regions in the PLS-DA analysis and regression coefficients were exploited to illustrate levels of metabolites in the regions. In addition, a non-parametric Wilcoxon rank sum test (P<0.05) was used for statistical comparison of these metabolites in anatomically different regions of metabolites with statistically significant differences between regions were created. *Homo sapiens*-associated pathway analyses were performed with significantly changed metabolites (P<0.05) using the Human Metabolome Database (Styczynski et al., 2007; Xia et al., 2012). MetaboAnalyst (Chong et al., 2019) and OmicsNet analysis software were used for pathway analysis of the metabolites that were significantly different between regions.

Quantification and statistical analysis

Statistical and graphical analyses were performed using MetaboAnalyst software, PASW Statistics (version 18.0.0.) and Microsoft Excel 2018. In the metabolomic analysis, a non-parametric Wilcoxon rank sum test (P<0.05) was used to determine the statistically significant different metabolites between the metabolome profiles of the R1 and R2 regions. Unless otherwise specified, a two-tailed Student's t-test was used to evaluate statistical significance, defined as P<0.05. Statistical analyses were performed depending on the spread of the variable as specified, and are reported as mean±s.d. Statistical details are included in the related results, figure legends and Materials and Methods.

Competing interests

The authors declare no competing or financial interests.

Author contributions

Conceptualization: S.A., D.U.C., R.K.O.; Methodology: S.A., E.N., D.U.C., S.K.; Software: S.A., E.N.; Validation: S.A., E.N.; Formal analysis: S.A., E.N., S.K.; Investigation: S.A.; Resources: S.A.; Data curation: S.A.; Writing - original draft: S.A.; Writing - review & editing: S.A., E.N., D.U.C., S.K., R.K.O.; Visualization: S.A.; Supervision: D.U.C., R.K.O.; Project administration: S.A., D.U.C., R.K.O.; Funding acquisition: S.A., E.N., D.U.C., S.K., R.K.O.

Funding

This work was supported by the Türkiye Bilimsel ve Teknolojik Araştirma Kurumu (TUBITAK; 213S006), the Scientific Research Projects Coordination Unit at Hacettepe Üniversitesi (013D09103001), and the TUBITAK Postgraduate Scholarship Program (2211-A-BIDEP to S.A.).

Data availability

The RNA-seq raw and analyzed data are available in GEO under accession number GSE145008.

Supplementary information

Supplementary information available online at
https://jcs.biologists.org/lookup/doi/10.1242/jcs.250720.supplemental

References

Abarrategi, A., Mian, S. A., Passaro, D., Rouault-Pierre, K., Grey, W. and Bonnet, D. (2018). Modeling the human bone marrow niche in mice: From host bone marrow engraftment to bioengineering approaches. *J. Exp. Med.* **215**, 729-743. doi:10.1084/jem.20172139

Ader, I., Brizuela, L., Bouquerel, P., Malavaud, B. and Cuvillier, O. (2008a). Sphingosine kinase 1: a new modulator of hypoxia inducible factor 1α during hypoxia in human cancer cells. *Cancer Res.* **68**, 8635-8642. doi:10.1158/0008-5472.CAN-08-0917

Ahmadzadeh, A., Kast, R. E., Ketabchi, N., Shahrabi, S., Shahjahani, M., Jaseb, K. and Saki, N. (2015). Regulatory effect of chemokines in bone marrow niche. *Cell Tissue Res.* **361**, 401-410. doi:10.1007/s00441-015-2129-4

Ahmadzadeh, A., Norozi, F., Shahrabi, S., Shahjahani, M. and Saki, N. (2016). Wnt/β-catenin signaling in bone marrow niche. *Cell Tissue Res.* **363**, 321-335. doi:10.1007/s00441-015-2300-y

Anthony, B. A. and Link, D. C. (2014). Regulation of hematopoietic stem cells by bone marrow stromal cells. *Trends Immunol.* **35**, 32-37. doi:10.1016/j.it.2013.10.002

Asri, A., Sabour, J., Atashi, A. and Soleimani, M. (2016). Homing in hematopoietic stem cells: focus on regulatory role of CXCR7 on SDF1a/CXCR4 axis. *EXCLI J.* **15**, 134-143.

Avigdor, A., Goichberg, P., Shivtiel, S., Dar, A., Peled, A., Samira, S., Kollet, O., Hershkoviz, R., Alon, R., Hardan, I. et al. (2004). CD44 and hyaluronic acid cooperate with SDF-1 in the trafficking of human CD34+ stem/progenitor cells to bone marrow. *Blood* **103**, 2981-2989. doi:10.1182/blood-2003-10-3611

Bahat, A. and Gross, A. (2019). Mitochondrial plasticity in cell fate regulation. *J. Biol. Chem.* **294**, 13852-13863. doi:10.1074/jbc.REV118.000828

Balduino, A., Mello-Coelho, V., Wang, Z., Taichman, R. S., Krebsbach, P. H., Weeraratna, A. T., Becker, K. G., de Mello, W., Taub, D. D. and Borojevic, R. (2012). Molecular signature and in vivo behavior of bone marrow endosteal and subendosteal stromal cell populations and their relevance to hematopoiesis. *Exp. Cell Res.* **318**, 2427-2437. doi:10.1016/j.yexcr.2012.07.009

Calvi, L. M. and Link, D. C. (2015). The hematopoietic stem cell niche in homeostasis and disease. *Blood* **126**, 2443-2451. doi:10.1182/blood-2015-07-533588

Cho, S.-Y., Lee, H.-J., Jeong, S.-J., Lee, H.-J., Kim, H.-S., Chen, C. Y., Lee, E.-O. and Kim, S.-H. (2011). Sphingosine kinase 1 pathway is involved in melatonin-induced HIF-1α inactivation in hypoxic PC-3 prostate cancer cells. *J. Pineal Res.* **51**, 87-93. doi:10.1111/j.1600-079X.2011.00865.x

Chong, J., Wishart, D. S. and Xia, J. (2019). Using metaboanalyst 4.0 for comprehensive and integrative metabolomics data analysis. *Curr. Protoc. Bioinform.* **68**, e86. doi:10.1002/cpbi.86

Chotinantakul, K. and Leeanansaksiri, W. (2012). Hematopoietic stem cell development, niches, and signaling pathways. *Bone Marrow Res.* **2012**, 270425. doi:10.1155/2012/270425

Cordeiro-Spinetti, E., Taichman, R. S. and Balduino, A. (2015). The bone marrow endosteal niche: how far from the surface? *J. Cell. Biochem.* **116**, 6-11. doi:10.1002/jcb.24952

Crane, G. M., Jeffery, E. and Morrison, S. J. (2017). Adult haematopoietic stem cell niches. *Nat. Rev. Immunol.* **17**, 573-590. doi:10.1038/nri.2017.53

Dias, S., Choy, M., Alitalo, K. and Rafii, S. (2002). Vascular endothelial growth factor (VEGF)–C signaling through FLT-4 (VEGFR-3) mediates leukemic cell proliferation, survival, and resistance to chemotherapy. *Blood* **99**, 2179-2184. doi:10.1182/blood.V99.6.2179

Ehninger, A. and Trumpp, A. (2011). The bone marrow stem cell niche grows up: mesenchymal stem cells and macrophages move in. *J. Exp. Med.* **208**, 421-428. doi:10.1084/jem.20110132

Ellis, S. L. and Nilsson, S. K. (2012). The location and cellular composition of the hemopoietic stem cell niche. *Cytotherapy* **14**, 135-143. doi:10.3109/14653249.2011.630729

Folmes, C. D. L., Dzeja, P. P., Nelson, T. J. and Terzic, A. (2012). Metabolic plasticity in stem cell homeostasis and differentiation. *Cell Stem Cell* **11**, 596-606. doi:10.1016/j.stem.2012.10.002

Friedlis, M. F. and Centeno, C. J. (2016). Performing a better bone marrow aspiration. *Phys. Med. Rehabil. Clin. N. Am.* **27**, 919-939. doi:10.1016/j.pmr.2016.06.009

Gao, X., Xu, C., Asada, N. and Frenette, P. S. (2018). The hematopoietic stem cell niche: from embryo to adult. *Development* **145**, dev139691. doi:10.1242/dev.139691

Grassinger, J., Haylock, D. N., Williams, B., Olsen, G. H. and Nilsson, S. K. (2010). Phenotypically identical hemopoietic stem cells isolated from different regions of bone marrow have different biologic potential. *Blood* **116**, 3185-3196. doi:10.1182/blood-2009-12-260703

Guarnerio, J., Coltella, N., Ala, U., Tonon, G., Pandolfi, P. P. and Bernardi, R. (2014). Bone marrow endosteal mesenchymal progenitors depend on HIF factors for maintenance and regulation of hematopoiesis. *Stem Cell Rep.* **2**, 794-809. doi:10.1016/j.stemcr.2014.04.002

Guerrouahen, B. S., Al-Hijji, I. and Tabrizi, A. R. (2011). Osteoblastic and vascular endothelial niches, their control on normal hematopoietic stem cells, and their consequences on the development of leukemia. *Stem Cells Int.* **2011**, 375857. doi:10.4061/2011/375857

Guezguez, B., Campbell, C. J. V., Boyd, A. L., Karanu, F., Casado, F. L., Di Cresce, C., Collins, T. J., Shapovalova, Z., Xenocostas, A. and Bhatia, M. (2013). Regional localization within the bone marrow influences the functional capacity of human HSCs. *Cell Stem Cell* **13**, 175-189. doi:10.1016/j.stem.2013.06.015

Hernigou, J., Picard, L., Alves, A., Silvera, J., Homma, Y. and Hernigou, P. (2014). Understanding bone safety zones during bone marrow aspiration from the iliac crest: the sector rule. *Int. Orthop.* **38**, 2377-2384. doi:10.1007/s00264-014-2343-9

Hu, X., Garcia, M., Weng, L., Jung, X., Murakami, J. L., Kumar, B., Warden, C. D., Todorov, I. and Chen, C.-C. (2016). Identification of a common mesenchymal stromal progenitor for the adult haematopoietic niche. *Nat. Commun.* **7**, 13095. doi:10.1038/ncomms13095

Itkin, T., Gur-Cohen, S., Spencer, J. A., Schajnovitz, A., Ramasamy, S. K., Kusumbe, A. P., Ledergor, G., Jung, Y., Milo, I., Poulos, M. G. et al. (2016). Distinct bone marrow blood vessels differentially regulate haematopoiesis. *Nature* **532**, 323-328. doi:10.1038/nature17624

Karaoz, E., Aksoy, A., Ayhan, S., Sarıboyacı, A. E., Kaymaz, F. and Kasap, M. (2009). Characterization of mesenchymal stem cells from rat bone marrow: ultrastructural properties, differentiation potential and immunophenotypic markers. *Histochem. Cell Biol.* **132**, 533-546. doi:10.1007/s00418-009-0629-6

Klamer, S. and Voermans, C. (2014). The role of novel and known extracellular matrix and adhesion molecules in the homeostatic and regenerative bone marrow microenvironment. *Cell Adhes. Migration* **8**, 563-577. doi:10.4161/19336918.2014.968501

Koenen, J., Bachelerie, F., Balabanian, K., Schlecht-Louf, G. and Gallego, C. (2019). Atypical chemokine receptor 3 (ACKR3): A comprehensive overview of its expression and potential roles in the immune system. *Mol. Pharmacol.* **96**, 809-818. doi:10.1124/mol.118.115329

Krause, D. S., Scadden, D. T. and Preffer, F. I. (2013). The hematopoietic stem cell niche—home for friend and foe? *Cytometry B Clin. Cytom.* **84B**, 7-20. doi:10.1002/cyto.b.21066

Lee, S.-H., Erber, W. N., Porwit, A., Tomonaga, M., Peterson, L. C. and **International councilfor standardization in hematology**. (2008). ICSH guidelines for the standardization of bone marrow specimens and reports. *Int. J. Lab. Hematol.* **30**, 349-364. doi:10.1111/j.1751-553X.2008.01100.x

Li, Z., Hao, J., Duan, X., Wu, N., Zhou, Z., Yang, F., Li, J., Zhao, Z. and Huang, S. (2017). The role of semaphorin 3A in bone remodeling. *Front. Cell. Neurosci.* **11**, 40. doi:10.3389/fncel.2017.00040

Lidgerwood, G. E., Pitson, S. M., Bonder, C. and Pébay, A. (2018). Roles of lysophosphatidic acid and sphingosine-1-phosphate in stem cell biology. *Prog. Lipid Res.* **72**, 42-54. doi:10.1016/j.plipres.2018.09.001

Lilly, A. J., Johnson, W. E. and Bunce, C. M. (2011). The haematopoietic stem cell niche: new insights into the mechanisms regulating haematopoietic stem cell behaviour. *Stem Cells Int.* **2011**, 274564. doi:10.4061/2011/274564

Lo Celso, C., Fleming, H. E., Wu, J. W., Zhao, C. X., Miake-Lye, S., Fujisaki, J., Côté, D., Rowe, D. W., Lin, C. P. and Scadden, D. T. (2009). Live-animal tracking of individual haematopoietic stem/progenitor cells in their niche. *Nature* **457**, 92-96. doi:10.1038/nature07434

Mendelson, A. and Frenette, P. S. (2014). Hematopoietic stem cell niche maintenance during homeostasis and regeneration. *Nat. Med.* **20**, 833-846. doi:10.1038/nm.3647

Miko, M., Danisovic, L., Majidi, A. and Varga, I. (2015). Ultrastructural analysis of different human mesenchymal stem cells after in vitro expansion: a technical review. *Eur. J. Histochem.* **59**, 2528. doi:10.4081/ejh.2015.2528

Muschler, G. F., Boehm, C. and Easley, K. (1997). Aspiration to obtain osteoblast progenitor cells from human bone marrow: the influence of aspiration volume. *J. Bone Joint Surg.* **79**, 1699-1709. doi:10.2106/00004623-199711000-00012

Nagasawa, T., Omatsu, Y. and Sugiyama, T. (2011). Control of hematopoietic stem cells by the bone marrow stromal niche: the role of reticular cells. *Trends Immunol.* **32**, 315-320. doi:10.1016/j.it.2011.03.009

Nemutlu, E., Zhang, S., Xu, Y.-Z., Terzic, A., Zhong, L., Dzeja, P. D. and Cha, Y.-M. (2015). Cardiac resynchronization therapy induces adaptive metabolic transitions in the metabolomic profile of heart failure. *J. Card. Fail.* **21**, 460-469. doi:10.1016/j.cardfail.2015.04.005

Nombela-Arrieta, C., Pivarnik, G., Winkel, B., Canty, K. J., Harley, B., Mahoney, J. E., Park, S.-Y., Lu, J., Protopopov, A. and Silberstein, L. E. (2013). Quantitative imaging of haematopoietic stem and progenitor cell localization and hypoxic status in the bone marrow microenvironment. *Nat. Cell Biol.* **15**, 533-543. doi:10.1038/ncb2730

Ochocki, J. D. and Simon, M. C. (2013). Nutrient-sensing pathways and metabolic regulation in stem cells. *J. Cell Biol.* **203**, 23-33. doi:10.1083/jcb.201303110

Palodetto, B., da Silva Santos Duarte, A., Rodrigues Lopes, M., Adolfo Corrocher, F., Marconi Roversi, F., Soares Niemann, F., Priscila Vieira Ferro, K., Leda Figueiredo Longhini, A., Melo Campos, P., Favaro, P. et al. (2017). SEMA3A partially reverses VEGF effects through binding to neuropilin-1. *Stem Cell Res.* **22**, 70-78. doi:10.1016/j.scr.2017.05.012

Park, D., Sykes, D. B. and Scadden, D. T. (2012). The hematopoietic stem cell niche. *Front. Biosci.* **17**, 30-39. doi:10.2741/3913

Patterson, T. E., Boehm, C., Nakamoto, C., Rozic, R., Walker, E., Piuzzi, N. S. and Muschler, G. F. (2017). The efficiency of bone marrow aspiration for the harvest of connective tissue progenitors from the human iliac crest. *J. Bone Joint Surg.* **99**, 1673-1682. doi:10.2106/JBJS.17.00094

Peck, B., Ferber, E. C. and Schulze, A. (2013). Antagonism between FOXO and MYC regulates cellular powerhouse. *Front. Oncol.* **3**, 96. doi:10.3389/fonc.2013.00096

Pleyer, L., Valent, P. and Greil, R. (2016). Mesenchymal stem and progenitor cells in normal and dysplastic hematopoiesis—masters of survival and clonality? *Int. J. Mol. Sci.* **17**, 1009. doi:10.3390/ijms17071009

Sánchez-Alcañiz, J. A., Haege, S., Mueller, W., Pla, R., Mackay, F., Schulz, S., López-Bendito, G., Stumm, R. and Marín, O. (2011). Cxcr7 controls neuronal migration by regulating chemokine responsiveness. *Neuron* **69**, 77-90. doi:10.1016/j.neuron.2010.12.006

Schofield, R. (1978). The relationship between the spleen colony-forming cell and the haemopoietic stem cell. *Blood Cells* **4**, 7-25

Shapiro, S. A. and Arthurs, J. R. (2017). Bone marrow aspiration for regenerative orthopedic intervention: technique with ultrasound guidance for needle placement. *Regen. Med.* **12**, 917-928. doi:10.2217/rme-2017-0109

Sharma, M. B., Limaye, L. S. and Kale, V. P. (2012). Mimicking the functional hematopoietic stem cell niche in vitro: recapitulation of marrow physiology by hydrogel-based three-dimensional cultures of mesenchymal stromal cells. *Haematologica* **97**, 651-660. doi:10.3324/haematol.2011.050500

Styczynski, M. P., Moxley, J. F., Tong, L. V., Walther, J. L., Jensen, K. L. and Stephanopoulos, G. N. (2007). Systematic identification of conserved metabolites in GC/MS data for metabolomics and biomarker discovery. *Anal. Chem.* **79**, 966-973. doi:10.1021/ac0614846

Suda, T. and Arai, F. (2008). Wnt signaling in the niche. *Cell* **132**, 729-730. doi:10.1016/j.cell.2008.02.017

Sudo, T. and Mizuno, H. (2018). [Dynamic analysis of hematopoietic stem cells in the bone marrow by intravital imaging.]. *Clin. Calcium* **28**, 231-236.

Sugimura, R., He, X. C., Venkatraman, A., Arai, F., Box, A., Semerad, C., Haug, J. S., Peng, L., Zhong, X.-B., Suda, T. et al. (2012). Noncanonical Wnt signaling maintains hematopoietic stem cells in the niche. *Cell* **150**, 351-365. doi:10.1016/j.cell.2012.05.041

Sugiyama, T., Kohara, H., Noda, M. and Nagasawa, T. (2006). Maintenance of the hematopoietic stem cell pool by CXCL12-CXCR4 chemokine signaling in bone marrow stromal cell niches. *Immunity* **25**, 977-988. doi:10.1016/j.immuni.2006.10.016

Szade, K., Gulati, G. S., Chan, C. K. F., Kao, K. S., Miyanishi, M., Marjon, K. D., Sinha, R., George, B. M., Chen, J. Y. and Weissman, I. L. (2018). Where hematopoietic stem cells live: the bone marrow niche. *Antioxid. Redox Signal.* **29**, 191-204. doi:10.1089/ars.2017.7419

Tamma, R. and Ribatti, D. (2017). Bone niches, hematopoietic stem cells, and vessel formation. *Int. J. Mol. Sci.* **18**, 151. doi:10.3390/ijms18010151

Tiziani, S., Kang, Y., Harjanto, R., Axelrod, J., Piermarocchi, C., Roberts, W. and Paternostro, G. (2013). Metabolomics of the tumor microenvironment in pediatric acute lymphoblastic leukemia. *PLoS ONE* **8**, e82859. doi:10.1371/journal.pone.0082859

Tjin, G., Flores-Figueroa, E., Duarte, D., Straszkowski, L., Scott, M., Khorshed, R. A., Purton, L. E. and Lo Celso, C. (2019). Imaging methods used to study mouse and human HSC niches: current and emerging technologies. *Bone* **119**, 19-35. 10.1016/j.bone.2018.04.022

Wang, A. and Zhong, H. (2018). Roles of the bone marrow niche in hematopoiesis, leukemogenesis, and chemotherapy resistance in acute myeloid leukemia. *Hematology* **23**, 729-739. doi:10.1080/10245332.2018.1486064

Wei, Q. and Frenette, P. S. (2018). Niches for hematopoietic stem cells and their progeny. *Immunity* **48**, 632-648. doi:10.1016/j.immuni.2018.03.024

Winkler, I. G., Sims, N. A., Pettit, A. R., Barbier, V., Nowlan, B., Helwani, F., Poulton, I. J., van Rooijen, N., Alexander, K. A., Raggatt, L. J. et al. (2010). Bone marrow macrophages maintain hematopoietic stem cell (HSC) niches and their depletion mobilizes HSCs. *Blood* **116**, 4815-4828. doi:10.1182/blood-2009-11-253534

Xia, J., Mandal, R., Sinelnikov, I. V., Broadhurst, D. and Wishart, D. S. (2012). MetaboAnalyst 2.0—a comprehensive server for metabolomic data analysis. *Nucleic Acids Res.* **40**, W127-W133. doi:10.1093/nar/gks374

Xie, Y., Yin, T., Wiegraebe, W., He, X. C., Miller, D., Stark, D., Perko, K., Alexander, R., Schwartz, J., Grindley, J. C. et al. (2009). Detection of functional haematopoietic stem cell niche using real-time imaging. *Nature* **457**, 97-101. doi:10.1038/nature07639

Xu, J., Sadahira, T., Kinoshita, R., Li, S.-A., Huang, P., Wada, K., Araki, M., Ochiai, K., Noguchi, H., Sakaguchi, M. et al. (2017). Exogenous DKK-3/REIC inhibits Wnt/β-catenin signaling and cell proliferation in human kidney cancer KPK1. *Oncology Lett.* **14**, 5638-5642. doi:10.3892/ol.2017.6833

Yuan, X., Logan, T. M. and Ma, T. (2019). Metabolism in Human Mesenchymal Stromal Cells: A Missing Link Between hMSC Biomanufacturing and Therapy?. *Front. Immunol.* **10**, 977. doi:10.3389/fimmu.2019.00977